FR 8800517

institut de physique nucléaire

LABORATOIRE ASSOCIÉ A L'IN2P3

UNIVERSITÉ PARIS-SUD

I.P.N. BP n° 1 - 91406 ORSAY

IPNO-DRE-87-13

SPECTROSCOPIC PROPERTIES OF TETRAVALENT ACTINIDE IONS IN SOLIDS

J.C. KRUPA

Laboratoire de Radiochimie - Institut de Physique Nucléaire B.P. N° 1 - 91 406 ORSAY France

SPECTROSCOPIC PROPERTIES OF TETRAVALENT ACTINIDE IONS IN SOLIDS

J. C. KRUPA

Laboratoire de Radiochimie - Institut de Physique Nucléaire
B.P. n° 1 - 91406 ORSAY (France)

ABSTRACT

Optical spectroscopy is a powerful tool to study the electronic structure of an optically active transition ion in the condensed phase media and consequently to study the interactions between the central ion and its environment. Up to now a great deal of efforts have been made in interpreting the energy levels of the 3^+ actinide ions diluted in different single crystal matrices using the successful parametric approach developed for the 3^+ lanthanides. The emphasis on An^{4+} is more recent and it is partly due to the development of new host materials such as $ThBr_4$, $ThCl_4$ and the already known $ThSiO_4$, that are characterized by a rather weak crystal field strength which makes possible the use of the same theoretical approach as for Ln^{3+}. Following this parametric model, the main interactions that are essential for an understanding of the energy level distribution of an f^N ion in solids is briefly examined and the deduced free-ion and crystal field parameters for Pa^{4+}, U^{4+}, Np^{4+} are compared to those of the isoelectronic configuration lanthanide ions.

At last, the actinide series offers an interesting situation since the 5f electrons in the metals are delocalized in the light actinides and then localized, that sould affect the nature of the chemical bonding in the two parts of the series. Is this trend reflected in the An^{4+} spectroscopic parameters ?

INTRODUCTION

The most important feature that characterizes the lanthanide and actinide elements is the small spatial extension of the open f shell which is under completion and then contains the optically active electrons. If these elements are engaged in compounds, the f electrons which belong to inner orbitals are well protected from the ligand interactions by the closed ns^2 np^6 external orbitals (n = 5 for lanthanides (4f) and n = 6 for actinides (5f)). Accordingly, the f electrons interact weakly with the electrons of neighbouring atoms and the electronic properties are only slightly affected by the environment. In particular, the solid state spectra of the 4 f and 5 f ions retain more or less their atomic character which is of great help in interpreting their level structure. In turn the small perturbation can be used to investigate the surrounding of the ion which then acts as a local probe.

However some differences exist between the two series. The 4f electrons are well localized and can be considered as core electrons with a small influence upon the binding which explains the dominant 3^+ oxidation state in the lanthanide series. In contrast, in the early actinides : Pa, U, Np, Pu and Am, the 5f orbitals tend to have a greater extension and consequently the contribution of the delocalized 5f electrons to the bonding is increased. The delocalization gives rise to a large variety of oxidation states leading to a large number of possible lowest electronic configurations (tab. 1) which is a characteristic of the first half-part of the actinide series. As the atomic number Z increases, the nuclear attraction stabilizes the 5f orbitals and the 5f electrons become more and more localized with a reduction of their bonding ability. From this point of view, the 5f electrons can be considered as an intermediate case between the 4f localized electrons and the 3d "extented" electrons which are very sensitive to their ligand environment.

A large fraction of our knowledge of the electronic states in solids has been obtained by optical spectroscopy and many important developments come from studies of the rare earth ions Ln^{3+} embedded in crystalline hosts (LaX_3, X = F, Cl, Br) (1,2 and ref. within). In the crystal, the metallic ion gives up the field-free spherical symmetry and comes under the influence of the inhomogeneous electrostatic field generated by the electrical charge distribution of the ligands. The crystal-field interaction removes the degeneracy of

the J states of the free-ion into a number of M_J crystal-field levels depending upon the symmetry of the environment which is the symmetry of the site occupied by the ion.

The knowledge of the symmetry of the crystal field is very helpful to interpret ion optical spectra. Through the group theory concepts based on symmetry properties (3), the crystal-field levels are associated to irreducible representations (Γ_n) belonging to the symmetry group under consideration. In addition to the number and degeneracy of crystal-field levels coming from each J level of the free-ion, the group theory methods permit to establish the selection rules which govern the transitions between these levels. In respect to the polarization properties of the light and the crystal orientation, the optical spectra reveal the nature and the multipolarity of the transitions (the dipolar electric transitions are the most intense unless and inversion center exists as symmetry element of the group).

For the Ln^{3+} and An^{3+}, An^{4+}, the lowest electronic configurations due to the lone non-closed f-shell are respectively $4\,f^n$ and $5\,f^n$ ($1 \leqslant n \leqslant 14$). Then, most of the observed transitions in the optical spectroscopy energy range, occur between crystal-field levels within f^n configurations. They are rather weak and sharp. This is a consequence of the Laporte selection rules stating that the electric dipole transitions between two states of the same parity are forbidden. Therefore the observed zero-phonon transitions in a non-centrosymmetric lattice site are forced electric dipole transitions (an inversion center causes the matrix element $\langle u \mid P \mid u' \rangle$ to be zero). This means that the f wavefunctions are not pure and contain contribution from excited opposite parity configurations. However these admixture, achieved through the odd terms of the hamiltonian describing the crystal-field interaction, is small enough to preserve the f character of the levels. Because of the decrease of configuration spacings due to the greater extension of the 5 f orbitals, the configuration interactions which mix wavefunctions with the same L and S is more pronounced in actinides than in lanthanides and the effect is expected to be more important for tripositive than for tetrapositive actinide ions.

A great deal of effort had been made in interpreting the spectra of the trivalent lanthanides (4, 5, 6, 7) and the corresponding actinides (8, 9, 10, 11) in lanthanum halide crystals especially. But as the actinide series offers an interesting situation due to the various oxidation states of the ions, the extension of the previous works was of great interest to test the crystal-field

model validity through the series for different ion charges and crystal-field strengths.

To explore the systematic trends, one needs crystalline hosts which on the one hand are optically inactive in the investigated energy range and on the other hand stabilize the selected oxidation state of the ion. Moreover the radii of the mutually substituted ions should be of the same size to avoid site distortions. In addition, the site symmetry should be high enough to facilitate the interpretation of the energy levels with the help of the selection rules. The development of new host materials offering these qualities such as $ThBr_4$ and $ThCl_4$ (12) gave a new impulse to An^{4+} spectroscopy, unfortunately limited by the reducing properties of the melt during the crystal growing. $ThSiO_4$ seems more promising.

Optical spectra of the f ions in solid state contain very often much more lines than expected from the splitting of the free-ion J levels. Apart the extra lines due to impurities and crystal lattice defects which change the site symmetry, some transitions called vibronics are generated by the coupling of electronic transitions with the vibration modes of the lattice. They are usually weaker and broader and they obey to different selection rules according to the space group representation. Temperature experiments are helpful to reveal the vibronic nature of these transitions especially for local symmetries showing and inversion center.

For non transparent compounds, the neutron spectroscopy, the paramagnetic resonance, the specific heat and the magnetic succeptibility are useful methods to investigate the splitting of the ground state multiplet but they are indeed sensitive when a few crystal-field levels are involved.

In the following section we shall stress the influence of the crystal field which modifies the energy levels and wavefunctions of the free-ion. But, as the free-ion levels are often unknown, the way of getting such information comes from theoretical considerations developed in the energy level calculations. The comparison of the energy levels obtained from the optical spectra to those calculated is the usual procedure to test the validity of the model under consideration.

ENERGY LEVEL CALCULATIONS

The energy level structure within the f^n configuration in condensed media may be understood in terms of the free-ion levels with an additional interaction due to the crystal field. Then the centers of gravity of all crystal-field level sets may be related to the free-ion degenerate J levels which are in turn related to the degenerate levels of the gaseous ion.

1. Free-ion

As starting point, in the central-field approximation, each electron is assumed to move independently in an undefined spherically symmetric potential originates from nucleus and other electron electrical charges. To overcome the difficulty arising from the unknown potential in the energy level calculation, one can use the parametric approach (13) based on the separation of the variables which characterize the acting potential. Following this procedure, the angular part of the interaction is totally evaluated from geometrical considerations while the radial integrals depending on the unknown potential are treated as parameters.

When the electrostatic and magnetic interactions between electrons are introduced, the Hamiltonian which describes the different interactions and then determines the f electron energy levels may be written as :

$$H = H_0 + H_{ER} + H_{SO} + H_{CORR}$$

where the first term H_0 represents the kinetic energy of the f electrons and their coulomb interaction with the nucleus through an effective nucleus charge Z^*

$$H_0 = -\frac{h^2}{2m} \sum_{i=1}^{n} \nabla^2_i - \sum_{i=1}^{n} \frac{z^* e^2}{r_i}$$

As H_0 contains only spin-independent spherically symmetric terms, it does not remove any degeneracy within the f^n configuration and therefore is not taken into consideration.

For systems of two or more f electrons, the mutual electron-electron electrostatic repulsion, H_{ER}, splits the configuration into terms characterized by ^{2s+1}L according to the spin multiplicity and the total angular momentum L (table 2). The simplest form of this effective hamiltonian into the framework of the parametric approach which considerers the undefined radial part as a parameter, may be written as :

$$H_{ER} = \sum_k F^k f_k \quad \text{with } k = 0, 2, 4, 6 \text{ for f electrons} \quad (k \leq 2\,l \text{ and even})$$

where f_k is the angular part of the interaction which can be evaluated from the symmetry of the system and F^k the Slater radial integral parameters determined empirically via a fitting procedure of the experimental data.

The spin-orbit interaction (between two magnetic dipoles), H_{SO}, removes the degeneracy of the ^{2S+1}L terms into J levels of the free-ion characterized by L, S, J quantum numbers ($^{2S+1}L_J$). This Hamiltonian can be written :

$$H_{SO} = \sum_i \zeta(r_i)\, \hat{l}_i \cdot \hat{s}_i$$

with for an hydrogen-like system :

$$\zeta_{(r)} = \frac{h^2}{2\, m^2\, c^2} \quad \frac{1}{r} \quad \frac{\delta U(r)}{\delta r}$$

where U(r) is the undefined potential in which the electron moves. In the parametric approach the hamiltonian describing the spin-orbit interaction may be expressed as :

$$H_{SO} = \zeta_f\, A_{SO}$$

where A_{SO} is the angular part of the spin-orbit interaction and ζ_f the spin-orbit coupling constant adjusted to the experimental observed energies.

The model developed above gives the right order of magnitude of the parameters but it is not able to reproduce accurately all the experimental data. Somes discrepancies remain between calculated and observed values and therefore it is apparent that the F^k and ζ associated purely with f^n configuration, cannot absorb all the effects. A better fit requires the introduction of new terms in the effective hamiltonian. They are regrouped in H_{CORR} which represents higher order correction terms.

Rajnak and Wybourne (14) have shown that among the higher order electrostatically-correlated perturbations, the dominant effect is the configuration interaction which occurs between configurations of the same parity. It is a scalar two-body interaction which can be taken into account by additional two-electron operators through the following hamiltonian :

$$H_1 = \alpha L(L + 1) + \beta G(G_2) + \gamma G(R_7)$$

where α, β and γ are the parameters associated with the two-body interaction and $G(G_2)$, $G(R_7)$ are the Casimir operators for the groups G_2 and R_7.

By extension a three-body interaction (for system with $n \geq 3$) was formulated by Judd (15) Crosswhite et al. (16), via the T^k parameters associated with three-particle operators :

$$H_2 = \sum_k T^k t_k \quad \text{with } k = 2, 3, 4, 6, 7, 8$$

In addition to these coulomb interactions, Judd et al. (17) introduced higher order magnetic effects due to configuration interactions and based on the fact that the admixture of a f' state into a particular f state is spin dependent. The corresponding parameters are included in the following hamiltonian :

$$H_3 = \sum_k p^k p_k \quad \text{with } k = 2, 4, 6$$

Further corrections of relativistic origin are namely the spin-spin interaction and the interaction between the spin of one electron and the orbital motion of another, called the spin-other orbit interaction. They are both

represented by the Marvin integrals M^k

$$H_4 = \sum_k M^k m_k \quad \text{with } k = 0, 2, 4$$

In the three last hamiltonians H_2, H_3, H_4, the lower-case letters account for the angular part of the interactions.

Since the 5f electrons in the actinides are more engaged in relativistic effects than 4f electrons in lanthanides, those parameters are expected larger for 5f than 4f ion.

2. Crystal-field hamiltonian

The crystal field interaction removes to a certain degree the degeneracy of the free-ion levels. The magnitude of the splitting of a J multiplet has been first parametrized in the simplest way assuming a static electrostatic field generated by the ion surrounding. In the crude charge point model (CPM) the ligand charges are supposed concentrated at the crystallographic position of the ions. A more realistic approach considers the charge density $\rho(R)$ of the environment to calculate the potential energy of a f electron :

$$V(r) = - \int \frac{e\rho(R)dr}{(R-r)}$$

when R is the distance to a particular point of the environment and r is the distance of the electron.

According to the parametric approach, it is convenient to write the potential V(r) in terms of B_q^k parameters with the Wybourne (18) formalism. The sum over the i electrons may be written as :

$$V_{CP} = \sum_{k,q,i} B_q^k \, C_q^k (\theta_i, \varphi_i)$$

where B_q^k are the crystal-field parameters (radial integrals)

$$B_q^k = - e \int (-1)^q \rho(R) \, C_{-q}^k (\theta, \varphi) \, \frac{r^k <}{r >^{k+1}} \, d\tau$$

and C_q^k are tensor operators of rank k for the angular part of the crystal-field interaction.

The k and q values are determined in consideration of the symmetry of the site occupied by the f ion and are limited by the requirement that the crystal-field potential is invariant under the symmetry operations of the group. The crystal-field interaction mix states with different J values.

It is also possible to define equivalence classes of noninteracting sets of states characterized by different crystal quantum numbers μ defined as :

$$\mu = M_J \text{ (modulo } n)$$

where n is the order of the higher rank symmetry operator C_n or S_n (see Table 3).

It must be remenbered that the electrostatic model is based upon the following assumptions which make it mathematically practicable : the crystal field is one-electron interaction which means that the f electron are independent of each other and the crystal-field operator is defined within the limited space of free-ion spin-orbitals of unpaired electrons only.

This brief review of the parametric energy level calculations of an f^n ion in solid state is summarized in table 4 where appeared together the different adjustable parameters to be evaluated from experimental data by a least-squares fitting procedure. If the experimental data amount is not sufficient to support analyses in which all the listed parameters are varying freely, the higher order correction parameters can be held fixed (for M^k, identical to those computed using HF methods for example) or some parameter values can be constrained by fixing ratios to be held constant. The parametrization scheme of the total hamiltonian reported here is able to reproduce satisfactorily the energy level structure of Ln^{3+} (19,20) but interpretative problems remain for the 5f electron systems especially for An^{4+} for which the standard deviations are appreciably larger. This acceptable agreement nevertheless says nothing about the validity of the model. As it was already pointed out, the different parameters absorb a variety of combined effects and the B_q^k, for instance, describe the crystal field interaction only in a global way. The leading contributions such as electrostatic, covalency and overlap effects are difficult to evaluate separately.

A priori calculations of crystal-field parameters are now often carried out using the superposition model developed by Newman (21). This model is based on the assumption that the total crystal-field potential is a sum of separate contributions from each of the ion in the crystal. Introduction of the overlap (22) between f and ligand orbitals as a consequence of the non-orthogonality of the free-ion wavefunctions and the covalency effect (22,24) due to charge transfer processes have provided better basis for the ab initio-calculations. In addition to these contact interactions, contributions from closed shells, referred as shielding effects (25) and the ligand polarizability (26) are also considered as well as the ligand-ligand electron exchange potential.

The superposition model calculations including all of these contributions provide crystal-field parameter sets which can be used to test the consistency of the experimentally evaluated parameters.

For further details about the theoretical considerations outlined in this section, one can refer to a number of books : Dieke (1), Ballhausen (27), Wybourne (18), Hüfner (28), Judd (29), Nielson and Koster (30), Jorgensen (31).

TETRAVALENT ACTINIDE OPTICAL SPECTROSCOPY

Among the tetravalent actinide ions, U^{4+} is the most widely studied ion due to several reasons. First, the low-level radioactivity of uranium natural isotopes makes the doped single crystals easy to handle without any special precautions which is absolutly not the case for all the other actinides except thorium. In addition to this there is no limitation for the sample size and no noticeable radiation effects. These factors, conjugated to the fact that U^{4+} oxidation state in compounds is stable or easy to stabilize in selected optically clear hosts, set U^{4+} ions well apart from the other actinide tetravalent ions. Moreover, the f^2 configuration of U^{4+} provides experimental features in sufficient details to be suitable for theoretical analysis and to constitute useful basis for extending the interpretation of spectra in condensed media. Recent U^V gaseous free-ion analysis [32,33], rather sparse for An^{4+} ions, magnifies the knowledge of U^{4+} energy level structure and provides instructive correlations between free-ion and crystal spectra.

The situation has so far been less successful for the other An^{4+}. It results in a lack of suitable matrices into which the 4^+ oxidation state can be stabilized. The promising $ThCl_4$ and $ThBr_4$ single-crystal hosts (which have to be compared to $LaCl_3$ and $LaBr_3$ for Ln^{3+} studies) brought interesting results for Pa^{4+} ($5f^1$) and U^{4+} ($5f^2$) but have failed for Np^{4+} ($5f^3$) where both 4+ and 3+ oxidation states were present compromising the reliability of the level assignment. $ThSiO_4$ and $ZrSiO_4$ hosts - with some restriction due to the smaller Zr^{4+} radius - seem more appropriate to investigate the whole series but a limitation arises from the flux crystal-growing technique which requires appreciable quantities of radioactive and expensive isotopic materials. As for Cs_2ThX_6 (X = Cl, Br) matrices, the presence of an inversion center in the octahedral lattice symmetry makes the analysis of the almost pure vibronic spectra difficult, without the usual aid of the polarization effect. The actinide borohydrides $X(BH_4)_4$ and borodeuterides $X(BD_4)_4$ with X = Pa^{4+}, U^{4+}, Np^{4+}... diluted in $Hf(BH_4)_4$ have also been successfully prepared but their optical spectra show rich vibronic structure which may mask pure electronic spectral features. An attempt has also be made with $PbMoO_4$ host doped with Np^{4+}, but as Np^{4+} substitutes into Pb^{2+} site, charge compensation is required and site distortion should occur. For the pure coloured An^{4+} compounds, part of the difficulty lie in the strong absorption of the photons which can be overcome by adjusting the thickness of the sample prepared for transmission spectroscopy. Organometallic compounds [$(Et_4N)_4An(NCS)_8$, Cp_3AnCl ($Cp=C_5H_5$),...] fall into this category.

Most of the optical results presented herein were obtained in β-$ThBr_4$, β-$ThCl_4$ and $ThSiO_4$ host lattices. At room temperature the three crystals have a D^{19}_{4h} tetragonal structure ($I4_1/amd$) isostructural with UCl_4. In this structure the Th^{4+} ion is at a site of D_{2d} symmetry and according to the higher value of the Th^{4+} radius, the other An^{4+} ion can substitute into this site without any site distortion. A displacing phase transition was observed in β-$ThBr_4$ and β-$ThCl_4$ respectively at 95 K and 70 K [34] by Raman spectroscopy. Neutron diffraction experiments [35] revealed that the low temperature structure is incommensurate along the C_4 axis with a modulation of the halide-ion distances in a plane perpendicular to this axis. The sinusoidal distortion reduces the actinide ion site symmetry from D_{2d} to D_2 with a continuous distribution of the different classes of site between the two limiting symmetries [36]. Laser selective site excitation experiments were able to sort out the respective absorption bands in D_{2d} and D_2 symmetries [37,38].

Beyond these matrix considerations, it should be pointed out before going further into details that for An^{4+} just as well in An^{3+} the crystal - field interaction cannot be considered as only a perturbation and therefore the total hamiltonian must be diagonalized simultaneously. The J-mixing of the wavefunctions is then properly accounted for. Furthermore, owing to the strong spin-orbit coupling, wavefunctions are no longer pure Russel-Saunders wavefunctions but a linear combination of them. However we will keep Russell-Saunders designation to give the largest contribution to the total wavefunction even if sometimes the mixing is so strong that the label is meaningless. Though intensity analysis will not be considered here, it is interesting to note that the absolute oscillator strengths of 5f transitions of U^{4+} in $ThBr_4$ and hydrobromic acid solution was found to be two order of magnitude larger than those of 4f transitions and ten times larger than for U^{3+} [39]. The absorption spectra of an^{4+} in solution (fig. 1) were of great help in interpreting the spectra in condensed media especially in the weak field cases.

PROTACTINIUM ION : Pa^{4+} ($5f^1$)

Only a few works are dealt with the optical spectroscopy of Pa^{4+} whose radioactivity represents a severe constraint. Data concerning optical and magnetic properties of Pa^{4+} doped into Cs_2ZrCl_6 were first reported by Axe [40] in an octahedral crystal-field symmetry. In protactinium compounds, $(Net)_2PaBr_6$ and $(Net)_2PaCl_6$, Edelstein et al [41] have fitted optical data in a similar octahedral field and Amberger et al [42] reported data for $PaCl_4$ in D_{2d} symmetry. But all these works were based on insufficient amount of experimental data and least-squares fitting can be justified only when the number of energy levels to be fitted exceeds the number of parameters ; otherwise the parameters will be overdetermined.

In the case of $Pa^{4+}:\beta$-$ThBr_4$ and $Pa^{4+}:\beta$-$ThCl_4$ [43,44], strong fluorescence was used to determine the energy of the low-lying stark levels of the ground state $^2F_{5/2}$. Consequently all the seven doubly degenerate Kramers crystal-field levels into which the $5f^1$ configuration of Pa^{4+} splits under the influence of the spin-orbit and crystal-field interactions, were experimentally measured in the infra-red region (fig. 2). The assigned spectra characterized by two irreducible representations Γ_6 and Γ_7 of double group associated with D_{2d} symmetry, were fit by a least squares routine to the

parameters of the following hamiltonian :

$$H = \zeta\ l.s + B_0^2 C_0^2 + B_0^4 C_0^4 + B_0^6 C_0^6 + B_4^4 (C_4^4 + C_{-4}^4) + B_4^6 (C_4^6 + C_{-4}^6)$$

The best fit is reported in table 5. Table 6 shows the six corresponding parameter values.

In the visible and near UV region, the intense emission spectra of Pa^{4+}:β-$ThBr_4$ and Pa^{4+}:β-$ThCl_4$ when irradiated with the 337.1 nm nitrogen laser line were assigned to 6d → 5f parity-allowed transitions in Pa^{4+} [45]. A tentative energy level scheme (fig. 3) was derived from the spectra but the entire energy spread of the 6d band appears to narrow and a missing level in the higher UV range should be found.

The radioluminescence (due to α and γ activities) which occurs in these crystals resembles in its intensity distribution among its spectral lines to that observed in UV excitation, suggesting that the primary excitation in radioluminescence takes place in the lattice.

URANIUM ION : U^{4+} ($5f^2$)

New interest in the study of U^{4+} in solid state started with the successful parametric analysis of U^{4+} in β-$ThBr_4$ [46] dealing with D_{2d} symmetry. On this basis, new interpretation of energy level structure of U^{4+} at a site of D_{2d} symmetry in the isomorphic $ThSiO_4$, β-$ThCl_4$ and UCl_4 has led to consistent sets of parameters when earlier published fits [47–57] were all quite tentative without any systematic trends.

Among the operations of the D_{2d} group of symmetry, there is no inversion center and then zero-phonon transitions were expected. The $\sigma(\vec{E} \perp \vec{C_4}$ and $\alpha(\vec{E}, \vec{H} \perp \vec{C_4})$ spectra were checked to be the same, which according to the transformation properties of electric-dipole operator, requires the use of electric dipole selection rules. In all the investigated compounds with a D_{2d} site, a Γ_4 ground state for U^{4+}, was assigned which is consistent with the selection rules and MCD experiments which proved the ground state to be a non-degenerate level [58] :

$\Gamma_4 \rightarrow \Gamma_1$ transitions are then observed on a π spectra ($\vec{E} \,//\, \vec{C_4}$) and $\Gamma_4 \rightarrow \Gamma_5$ transitions on σ spectra ($\vec{E} \perp \vec{C_4}$).

Among the four systems, the U^{4+}: $ThSiO_4$ spectra [59] are the simplest with narrow lines and few vibronic components. The spectra get more complex with U^{4+}: $ThBr_4$ [46], U^{4+}: $ThCl_4$ [60] and UCl_4 [61]. In β-TBr_4 and β-$ThCl_4$ the presence of an infinity of very close environments for the U^{4+} ions due their incommensurate structures at low temperature, induces a broadening of the spectroscopic lines which can reach an appreciable width (up to $100cm^{-1}$ for some $\Gamma_4 \rightarrow \Gamma_5$ transitions). In UCl_4, the broadening comes from the interactions between uranium ions and a marked vibronic structure. Despite the above mentioned differences the similarity of those spectra is a striking feature (fig. 4,5).

The experimental levels were fitted by simultaneous diagonalization of the free-ion and crystal-field hamiltonians characterized by the parameters of

- Interelectronic repulsion : F^k ($k = 2, 4, 6$)
- Spin-orbit coupling : ζ
- Configuration interactions : α, β, γ
- electrostatically correlated spin-orbit interactions : P^k ($k = 2,4,6$)
- spin-spin and spin other-orbit interactions M^k ($k = 0,2,4$)
- crystal-field interactions : B_0^2, B_0^4, B_4^4, B_0^6 and B_4^6

The better fit led to the parameters listed in table 7. It should be noticed that the energy levels are not very sensitive to the value of B_4^6 parameter and then it appears always poorly determined.

In D_2 symmetry, encountered also in U^{4+}: ThX_4 (X = Br, Cl) at low temperature, supplementary crystal-field parameters have to be added to account for the symmetry lowering : B_2^2, B_2^4 and B_6^6. The obtained parameter values are reported in table 8.

It should be emphasized that ThX_4 (X = Cl, Br) is one of the few matrices along with $ThSiO_4$ where U^{4+} is known to fluorese in solid state.

Special interest was brought to UCl_4 which has been studied more in detail [52,53,60]. In particular the $^3H_4$ ground manifold splitting was investigated by different methods : magnetic succeptibility [62] and neutron inelastic scattering [63, 64] in order to establish the energy of the low-lying crystal-field levels. A priori calculations of the crystal-field parameters

performed according to the superposition model have shown the importance of nonorthogonality and covalency effects [65]. The difference between the experimental and calculated value of B_0^2 parameter suggested that the electrostatic polarization of the whole crystal-lattice cannot be ignored.

One has to mention the recent work on α-$ThBr_4$ host (space group $I4_1/a$) in which U^{4+} ions in S_4 local symmetry fluoresce strongly [66].

More extensive analysis of the spectra of U^{4+} have been published in higher symmetries, T_d and O_h, respectively in $U(BD_4)_4/Hf(BD_4)_4$ [67] and crystals containing UX_6^{2-}(X = Cl, Br) complexes such as Cs_2UCl_6 [68]. The largest crystal-field splitting and the consecutive higher B_q^k parameter values (table 9) found for these two symmetries stand in contrast with the parameter values determined for U^{4+} in the D_{2d} symmetry of $ThBr_4$, $ThCl_4$, $ThSiO_4$ and UCl_4 which are characterized by a rather weak field interaction (fig. 6).

To compare the magnitude of the different crystal-field strengths, it is convenient to use a scalar crystal-field parameter introduced by Auzel [69] and expressed as :

$$N_v / (4\pi)^{1/2} = [\sum_{k,q} (B_q^k)^2 / 2k + 1]^{1/2}$$

N_v is a number which characterizes the crystal-field strength in any kind of site symmetry and then permits cross-comparison between different crystals.

In octahedral crystalline field, since the dipolar electronic transitions are forbidden because of inversion center, the U^{4+} absorption spectra are essentially vibronic with several weak magnetic dipole transitions. As actinides couple much more than lanthanides with the lattice, actinides generally display rich vibronic spectra. The observed pure electric transitions are associated to a local distortion caused by lattice imperfections. The parametric analysis results in r.m.s. deviation greater than 100 cm^{-1} (one order higher than those obtained in lanthanides). The parameters obtained by Satten et al. [68] for the hexachloro complex are listed in table 9.

Uranium organometallic compounds have, up to now, never been really successfully assigned [70-72]. The general disagreement could be attributed to a lack of oriented crystals or a use of approximate symmetries to

characterize inequivalent sites which arise in salts containing large cation complexes.

NEPTUNIUM ION : $Np^{4+}(5f^3)$

Formally, the Np^{4+} crystal energy level structure is equivalent to its lanthanide analogue $Nd^{3+}(4f^3)$ but the interpretation of optical data has led to the conclusion that the comparison is not so straightforward. The larger spin-orbit coupling combined to larger crystal-field interactions on one hand mix strongly the SLJ character of the levels and on the other hand induce important overlappings of the excited crystal-field levels as the energy increases (fig. 7). Because of this high density of states, only the stark components of the four lowest manifolds, $^4I_{9/2}$, $^4I_{11/2}$, $^4F_{3/2}$ and $^4I_{13/2}$, which are well-isolated can be reasonably assigned and fitted for parametric analysis in condensed media. As the crystal-field splitting is smaller than the quadruplet separation, J can be considered as a good quantum number for these four manifolds. Fluorescence occurs generally from quadruplet $^4I_{11/2}$, therefore the ground state structure which cannot be found through absorption, can be well determined as it was shown for $Np^{4+}:PbMoO_4$ [73] and $Np^{4+}:ThSiO_4$ [74] systems. Exceptionally, in the visible region, the relatively pure $^4G_{7/2}$ manifold situated on one side of an energy gap can be accurately assigned, increasing validly the small amount of reliable experimental data to be fitted.

In $Np^{4+}:ThSiO_4$, the D_{2d} crystal-field symmetry splits the free-ion J levels into kramers doublets designated by Γ_6 and Γ_7 irreducible representations of the D_{2d} group. They are associated respectively with the crystalline quantum numbers $\mu = 1/2$ and $\mu = 3/2$. The diagonalization of the full hamiltonian including the three-body configuration interaction parameters $F^k(k = 2,3,4,6,7,8)$ followed by the usual least-squares fitting procedure has provided the parameters listed in table 10. 29 levels were assigned with a r.m.s. of 46 cm^{-1}. The comparison with the crystal-field parameters obtained for U^{4+}: $ThSiO_4$ shows some discrepencies, especially for B_0^2 but the positive sign accounts for the polarization of the $^4F_{3/2}$ manifold.

In an earlier work, energy level structure of Np^{4+} in $PbMoO_4$ [73] was investigated in a S_4 local symmetry which is a subgroup of D_{2d}. The absorption and emission regions are quite similar in both crystals but $ThSiO_4$ provided more detailed spectra. Calculations involving only the five lowest

multiplets were based on a first order crystal-field model with initial free-ion parameters values proposed by Conway [75] (interpreting Np^{4+} spectra in solution [76]) and without including J mixing. However this attempt represents the first important contribution to Np^{4+} spectroscopy in solid state.

$Np^{4+}:ZrSiO_4$ study was also recently undertaken, in D_{2d} symmetry [77]. Though the main features are identitical to those recorded on $Np^{4+}:ThSiO_4$, the fitted parameters (table 10) are surprisingly different. The large discrepencies in the B_q^k values enlighten the difficulties encountered with Np^{4+} ion spectroscopy which will remain for a while, an open field for further investigations.

Example of higher symmetry cases was provided by the extensively studied $Np(BD_4)_4/Zr(BD_4)_4$ system [78]. In the Td symmetry, Np^{4+} ion levels are designated by Γ_6, Γ_7 and Γ_8 irreducible representations with respective degeneracies 2, 2 and 4. As it was already pointed out for U^{4+} ions doped in the same host, the large number of vibronic transitions gives rise to many ambiguities in the identification of pure electronic transitions. Nevertheless, a very coherent determination of the parameter values was carried out by adopting comparative approaches. The first order free-ion parameter ranges were determined by assuming that the same differences exist between U^{3+} and Np^{3+} in $LaCl_3$ on one side and U^{4+} and Np^{4+} in $U(BD_4)_4$ and $Np(BD_4)_4$ on the other side. Constant differences were also assumed between the pseudo-relativistic Hartree-Fock calculated values and the parameter values determined from $U(BD_4)_4$ and $Np(BD_4)_4$. A total of 46 zero-phonon transitions were assigned and fitted with a r.m.s. of 84 cm^{-1}. The obtained parameters are listed in table 10.

In octahedral and cubic crystal fields, data were published for Cs_2NpCl_6 [79], $[(C_2H_5)_4N]_2\ NpCl_6$ [80] and ThO_2 [81] where Np^{4+} ions occupy a site of inversion symmetry. The recent $Np^{4+}:ThO_2$ analysis [74] has shown the vibronic character of the spectra in contradiction with the previous work [81] where small distortions removing the inversion centre were supposed in order to allow weak forced electric dipole transitions. Only 16 accurate levels were considered which is far not enough, in regards to the parameter number, to describe fully the energy levels of Np^{4+}. Thus, just a tentative fit which is certainly not unique, was proposed (table 10).

PLUTONIUM ION Pu^{4+} ($5F^4$) AND HEAVIER An^{4+}

While for tetravalent actinide, spectra of the aquo-ions or in solid state (usually XF_4) have been obtained for many years up to Cf^{4+} (fig. 1) reliable parameter values for the heavier An^{4+} are rather sparse, even for Pu^{4+}.

Recently, Pu^{4+}: $ThSiO_4$ and Am^{4+}: $ThSiO_4$ crystals were grown with the flux technique and polarized absorption spectra were recorded for Pu^{4+} ion (fig. 8). Preliminary calculations, using parameters deduced from Np^{4+}: $ThSiO_4$, reproduce fairly well the main features as the absorption regions and the energy gaps.

Futhermore, anhydrous solid americium tetrafluoride $^{241}AmF_4$, was prepared [82] as well as CmF_4 [83], BkF_4 [84] and CfF_4. Absorption spectra of these fluorides were recorded and fluorescence was recently observed for $^{249}Bk^{4+}$ in CeF_4 [85].

Attempts to interpret some of these spectra were already published [86,87] but the results should be considered preliminary and certainly many works remained unpublished because of a lack of valuable basis. For these reasons, the predictive model proposed by H.M. Crosswhite, H. Crosswhite and W.T. Carnall [11, 13, 88, 89] is of great importance.

THE C.C.C. PREDICTIVE MODEL

The systematic interpretation of the trivalent lanthanide and actinide spectra has shown that the trend in the fitted values of F^k and ζ free-ion parameter, as a function of the atomic number Z, follows roughly the variation of the corresponding calculated Hartree-Fock values [90]. The variations are not linear, but the difference between the two sets of values, versus Z, appears nearly constant over the whole series (table 11). Thus, if the analysis of one element of the series has provided reliable parameters, the extrapolation procedure proposed by the model can predict the energy level structure of the other members.

This model was applied to calculate the An^{4+} ion energy level diagrams (fig. 9) using the $ThX_4:U^{4+}$ parameter values as basis for the weak crystal-field case (table 12). Concerning this point, one can notice that $U^{4+}:ThBr_4$ absorption spectrum is well correlated to the observed spectrum for U^{4+}_{aquo} (fig. 10).

This new approach is very useful to test the accuracy of experimentally determined parameter values or to provide first sets of parameters to initiate the calculations.

COMPARISON BETWEEN ACTINIDES AND LANTHANIDES

When the parameters issued from the $5f^n$ ion parametric analyses are compared to those obtained for the $4f^n$ ions for configurations with the same number of f electrons (table 13), the striking features are :

- the reduction of the F^k slater parameters (fig. 11)
- the large increase of the spin-orbit coupling constant (fig. 12)
- the larger crystal-field parameters (fig. 13).

Because of the reduction of the electronic repulsion, the energy ranges for $5f^n$ configurations are reduced when the larger spin-orbit and crystal-field interactions shorten the energy gaps between J levels. Then, overlappings and density of levels increase considerably with excitation energy (fig. 14) and consequently J levels for An^{4+} ions order differently than for the corresponding Ln^{3+}.

Furthermore the larger ζ values mix more the S, L character of An^{4+} levels. In addition, the admixing of J states due to larger B^k_q values, becomes greater and reduces the selection rule effects. Simultaneously, the odd crystal-field parameters induced comparatively larger admixing of opposite parity states into $5f^n$ configuration increasing the intensity of the forced electric dipole transitions.

The dynamic crystal-field interactions and ion-phonon coupling will also be greater for the actinides, increasing the probability for vibronic transitions.

The comparison between the Hartree-Fock calculated values for Ln^{3+} and An^{4+} and those empirically determined from optical spectra in solid state shows also some more trends. The difference for F^2 parameter values (fig. 10) is due essentially to the combination of two effects : the configuration interaction and to a less amount, the depression of high levels by the crystal environment [91]. But, as it was already pointed out, the 5f orbitals are more extended than 4f and thus one can expect more configuration interaction and a greater sensitivity to the crystal field for An^{4+}. These two factors explain the larger reduction of F^2 for An^{4+} than for Ln^{3+} while F^4 and F^6 which are less affected by the configuration interaction are less reduced. The particular crystal-field effect underlined above is expected to be magnified in the high symmetry cases, O_h and T_d, where the crystal-field strengths are approximatively twice as large as those found for the lower symmetry D_{2d}. The F^k values determined for U^{4+} ions respectively in Cs_2UX_6 (X = Cl, Br), $U(BD_4)_4$ and ThX_4(X = Cl, Br) show this evolutive trend : the F^k values increase as the crystal-field strength decreases (tables 7, 9).

For the parameters F^k and ζ, the difference between their values for the free-ion and the ion in the solid state is often referred to the nephelauxetic effect [92]. The ratio $\beta = F^2_{crystal}/F^2_{free\text{-}ion}$ can be used as a measure of the effect and provides an indication of the degree of covalency in the ion-bonding. Indeed, the nephelauxetic series, in terms of the magnitude of the effect for inorganic compounds can be expressed as :

$$\text{Free-ion} < F^- < O^{2-} < Cl^- < Br^- < I^- \simeq S^{2-} < Se^{2-} < Te^{2-}$$

which is equivalent to the ionicity or covalency ordering (F^- being the least covalent ion).

This order is well reproduced for the β ratio found in U^{4+}: $ThSiO_4$, U^{4+}: $ThCl_4$ and U^{4+}: $ThBr_4$ which takes respectively the values 0.83, 0.82 and 0.81 [table 14]. The F^2 reduction makes the 5f electrons of U^{4+} act more like 3d than 4f electrons. But according to Newman [93], the nephelauxetic series cannot be determined by the degree of admixture between ligand and f open-shell wavefunctions and is related only to the ligand polarizability. His demonstration is based upon the fact that the spectrochemical series where the ligands are ordered by the magnitude of the crystal-field splitting, due essentially to overlap and covalency, is opposite to the nephelauxetic

ordering. The B_q^k values obtained for $Pa^{4+}:ThCl_4$ and $Pa^{4+}:ThBr_4$ [table 6] follow fairly well the spectrochemical series which can be expressed as :

$$\text{Free ion} < I^- < Br^- < Cl^- < S^{2-} < F^- < O^{2-}$$

Unfortunately it is not the case for U^{4+} in $ThBr_4$, $ThCl_4$, $ThSiO_4$ where any obvious trend appears.

For these reasons as well as for the relatively important standard deviation found in reproducing the An^{4+} optical data, there are some evidences that the crystal-field model is not able to account for all the effects and some more refinements are expected. Special attention has to be drawn to the fact that the standard deviation increases when the crystal-field strength becomes larger.

REFERENCES

1. G.H. DIEKE, Spectra and Energy Levels of Rare Earth Ions in Crystals, Interscience Publishers, John Wiley New-York (1968)

2. W.T. CARNALL, H. CROSSWHITE, H.M. CROSSWHITE, Energy Level Structure and Transition Probalities of the Trivalent Lanthanides in LaF_3, Argonne National Laboratory Report (1977)

3. G.F. KOSTER, J.O. DIMMOCK, R.C. WHEELER and H. STATZ, Properties of the Thirty-two-Point Groups, M.I.T. Press, Cambridge, Mass. (1963)

4. C.A. MORRISON and R.P. LEAVITT, J. Chem. Phys., 71(1979)2366

5. W.T. CARNALL, G.L. GOODMAN, R.S. RANA, P. VANDEVELDE, L. FLUYT and C. GORLLER-WALRAND, J. Less. Com. Metals, 116(1986)17

6. H.M. CROSSWHITE, Spectroscopie des Elements de Transition et des Eléments Lourds dans les Solides, Colloque Int. du CNRS (28 juin 1976) Edition du CNRS, Paris (1977)

7. P. PORCHER and P. CARO, J. Chem. Phys. 68(1978)4176

8. H. LAMMERMANN and J.G. CONWAY, J. Chem. Phys. 38(1963)259

9. J.B. GRUBER, W.R. COCHRAN, J.G. CONWAY and A.T. NICOL J. Chem. Phys. 45(1966)1423

10. W.T. CARNALL, H. CROSSWHITE, H.M. CROSSWHITE, J.P. HESSLER, N. EDELSTEIN, J.G. CONWAY, G.V. SHALIMOFF, R. SARUP, J. Chem. Phys. 72(1980)5089

11. W.T. CARNALL and H.M. CROSSWHITE, Optical Spectra of Actinide Ions in Compounds and in Solution, Argonne National Laboratory Report, ANL-84-90(1985)

12. M. HUSSONNOIS, J.C. KRUPA, M. GENET, L. BRILLARD and R. CARLIER,
J. of Crystal Growth 51(1981)11

13. H.M. CROSSWHITE and H. CROSSWHITE, J. Opt. Soc. Am., B1(1984)246

14. K. RAJNAK and B.G. WYBOURNE, Phys. Rev. 132(1963)280

15. B.R. JUDD, Phys. Rev., 141(1966)4

16. H. CROSSWHITE, H.M. CROSSWHITE and B.R. JUDD, Phys. Rev. 174(1968)89

17. B.R. JUDD, H.M. CROSSWHITE and H. CROSSWHITE, Phys. Rev. 169(1968)130

18. B.G. WYBOURNE, Spectroscopic Properties of Rare Earths, Interscience Publishers, New York (1965)

19. J.P. HESSLER and W.T. CARNALL, ACS Symposium Series n° 131(1980)349

20. F.S. RICHARDSON, M.F. REID, J.J. DALLARA and R.D. SMITH, J. Chem. Phys. 83(1985)3813

21. D.J. NEWMAN, Adv. Phys. 20(1971)197

22. O.L. MALTA, Chem. Phys. Letters 87(1982)27

23. B.R. JUDD, J. Phys. C : Solid St. Phys. 13(1980)2695

24. ELLIS and D.J. NEWMAN, J. Chem. Phys. 49(1968)4037

25. R.M. STERNHEIMER, M. BLUME and R.F. PEIERLS, Phys. Rev. 173(1968)376

26. M.T. HUTCHINGS and D.K. RAY, Proc. Phys. Soc. (London) 81(1963)663

27. C.J. BALLHAUSEN, Introduction to Ligand Field Theory, McGraw-Hill, Series in Advanced Chemistry, New-York (1962)

28. S. HUFNER, Optical Spectra of Transparent Rare Earth Compounds, Academic Press, New-York (1978)

29. B.R. JUDD, Operators Techniques in Atomic Spectroscopy, Mc-Graw-Hill, New-York (1963)

30. C.W. NIELSON and G.F. KOSTER, Spectroscopic Coefficients for the p^n, d^n and f^n configurations, MIT Press, Cambridge, Mass (1963)

31. C.K. JORGENSEN, Absorption Spectra and Chemical bonding in complexes, Pergamon Press London (1962)

32. J.F. WYART, V. KAUFMAN and J. SUGAR, Phys. Scr. 22(1980)389

33. C.H.H. VAN DEURZEN, K. RAJNAK and J.G. CONWAY, J. Opt. Soc. Am. B1(1984)45

34. S. HUBERT, P. DELAMOYE, S. LEFRANT, M. LEPOSTOLLEC and M. HUSSONNOIS, J. Solid State Chem. 36(1981)36

35. L. BERNARD, R. CURRAT, P. DELAMOYE, C.M.E. ZEYEN, S. HUBERT, R. DE KOUCHKOVSKY, J. Phys. C16(1983)433

36. P. DELAMOYE and R. CURRAT, J. Phys. Letters 43(1982)655

37. P. DELAMOYE, J.C. KRUPA, J.G. CONWAY and N. EDELSTEIN, Phys. Rev. B28(1983)4913

38. J.C. KRUPA, C. KHAN MALEK, P. DELAMOYE, B. MOINE and C. PEDRINI, Physica Status Solidi (b) 140 (1987) 289

39. F. AUZEL, S. HUBERT and P. DELAMOYE, J. Luminesc. 26(1982)251

40. J.D. AXE, Ph. D. Thesis UCRL (1960)

41. N. EDELSTEIN, D. BROWN and B. WHITTAKER, Inorg. Chem. 13(1974)563

42. H.D. AMBERGER, W. GRAPE and E. STUMPP, Actinides 1981, Asilomar Conf. Abst., L.B.L. 12441 (1981)

43. J.C. KRUPA, M. HUSSONNOIS, M. GENET and R. GUILLAUMONT, J. Chem. Phys. 77(1982)154

44. J.C. KRUPA, S. HUBERT, M. FOYENTIN, E. GAMP and N. EDELSTEIN, J. Chem. Phys. 78(1983)2175

45. R.C. NAIK and J.C. KRUPA, J. of Luminesc. 31,32(1984)222

46. P. DELAMOYE, K. RAJNAK, M. GENET and N. EDELSTEIN, Phys. Rev. B,28(1983)4923

47. I. RICHMAN, P. KISLIUK and E.Y. WONG, Phys. Rev. 155(1967)262

48. D.J. MACKEY, W.A. RUNCIMAN and E.R. VANCE, Phys. Rev. B11(1975)211

49. E.R. VANCE and D.J. MACKEY, Phys. Rev. B18(1978)185

50. E.R. VANCE and D.J. MACKEY, J. Phys. C7(1974)1898

51. E.R. VANCE and D.J. MACKEY, J. Phys. C8(1975)3499

52. R. McLAUGHLIN, J. Chem. Phys. 36(1962)2699

53. H.G. HECHT and J.B. GRUBER, J. Chem. Phys. 60(1974)4872

54. D.R. JOHNSTON, R.A. SATTEN, C.L. SCHREIBER and E.Y. WONG, J. Chem. Phys. 44(1966)3141

55. W.A. HARGREAVES, Phys. Rev. B, 2(1970)2273

56. R.A. SATTEN, C.L. SCHREIBER and E.Y. WONG, J. Chem. Phys. 42(1964)162

57. E.R. BERNSTEIN and T.A. KEIDERLING, J. CHEM. PHYS. 59(1973)2105

58. B. BRIAT, P. DELAMOYE, J.C. RIVOAL, S. HUBERT and P. EVESQUE, J. Physique 46(1985)1375

59. C. KHAN MALEK and J.C. KRUPA, J. Chem. Phys. 84(1986)6584

60. C. KHAN MALEK, J.C. KRUPA, P. DELAMOYE and M. GENET, J. de Physique 47(1986)1763

61. C. KHAN MALEK, J.C. KRUPA and M. GENET, Spectrochimica Acta 42A(1986)907

62. E. GAMP, N. EDELSTEIN, C. KHAN MALEK, S. HUBERT and M. GENET, J. Chem. Phys. 79(1983)2023

63. P. DELAMOYE, J.C. KRUPA, S. KERN, C.K. LOONG and G.H. LANDER, J. Less. Com. Metals. 122(1986)59

64. A. MURASIK, J. LECIEJEWICZ and Z. ZOLNIEREK, Phys. Stat. Sol. 80b(1977)

65. Z. ZOLNIEREK, Z. GAJEK and C. KHAN MALEK, Physica 125B(1984)199

66. S. HUBERT, E. SIMONI and M. GENET, J. Less Com. metals 122(1986)81

67. K. RAJNAK, E. GAMP, R. SHINOMOTO and N. EDELSTEIN, J. Chem. Phys. 80(1984)5942

68. R.A. SATTEN, C.L. SCHREIBER and E.Y. WONG, J. Chem. Phys. 78(1983)79

69. F. AUZEL and O. MALTA, J. Physique 44(1983)201

70. H.D. AMBERGER and G.R. SIENEL, Z. Naturforsch. 31b(1976)769

71. H.D. AMBERGER, J. Organomet., Chem. 116(1976)219

72. H.D. AMBERGER, R.D. FISCHER and K. YUNLU, Organometallics, in press

73. K.K. SHARMA and J.O. ARTMAN, J. Chem. Phys. 50(1969)1241

74. M.P. LAHALLE, J.C. KRUPA, R. GUILLAUMONT and C. RIZZOLI, J. Less Com. Met. 122(1986)65

75. J.G. CONWAY, J. Chem. Phys. 41(1964)904

76. W.C. WAGGENER, J. Chem. Phys. 62(1958)382

77. I. POIROT, W. KOT, G. SHALIMOFF, N. EDELSTEIN, M.M. ABRAHAM, C.B. FINCH and L. BOATNER, in preparation

78. K. RAJNAK, R.H. BANKS, E. GAMP and N. EDELSTEIN, J. Chem. Phys. 80(1984)12

79. E.R. MENZEL and J.B. GRUBER, J. Chem. Phys. 54(1971)3857

80. E.R. MENZEL, J.B. GRUBER and J.L. RYAN, J. Chem. Phys. 57(1972)4287

81. J.B. GRUBER and E.R. MENZEL, J. Chem. Phys. 50(1969)3772

82. L.B. ASPREY and R.A. PENNEMAN, Inorg. Chem. 1(1962)134

83. B.F. MYASOEDOV, I.A. LEBEDEV and V.M. MIKHAILOV, Dok. Akad. Nauk SSSR211(1973)1351

84. D.D. ENSOR, J.R. PETERSON, R.G. HAIRE and J.P. YOUNG, J. Inorg. Nucl. Chem.,43(1981)1001

85. G.M. JURSICH, J.V. BEITZ, W.T. CARNALL, G.L. GOODMAN, C.W. WILLIAMS and L.R. MORSS, to be published

86. L.P. VARGA, R.D. BAYBARZ, M.J. REISFELD and L.B. ASPREY, J. Inorg. Nucl. Chem. 35(1973)2775

87. L.P. VARGA, R.D. BAYBARZ, M.J. REISFELD and J.B. MANN, J. Inorg. Nucl. Chem. 35(1973)2303

88. W.T. CARNALL and H.M. CROSSWHITE in "The Chemistry of the Actinide Eléments" Vol.2 eds J.J. KATZ, G.T. SEABORG and L.R. MORSS, Chapman and Hall (London) 1986

89. W.T. CARNALL, J. Less. Com. Met. 122(1986)1

90. R.D. COWAN and D.C. GRIFFIN, J. Opt. Soc. Am., 66(1976)1010

91. K. RAJNAK, Private communication

92. C.E. SCHAFFER and C.K. JORGENSEN, J. Inorg. Nucl. Chem. 8(1958)143

93. D.J. NEWMAN, Aust. J. Phys., 30(1977)315

94. C. KHAN MALEK, J.C. KRUPA and M. GENET, Inorg. Chimica Acta 115(1986)115

95. J.C. CONWAY, J.C. KRUPA, P. DELAMOYE and M. GENET, J. Chem. Phys. 74(1981)849

96. T. HAYHURST, G. SHALIMOFF, J.G. CONWAY, N. EDELSTEIN, L.A. BOATNER and M. ABRAHAM, J. Chem. Phys. 76(1982)3960

97. D.L. WOOD, J. FERGUSON, K.R. KNOX and J.F. DILLON, J. Chem. Phys. 39(1963)890

FIGURE CAPTIONS

Fig. 1 : Absorption spectra of tetravalent actinides in solution or solid state (from W.T. Carnall and H.M. Crosswhite [11] and ref. within)

Fig. 2 : Energy level diagram for $Pa^{4+}:ThBr_4$ and $Pa^{4+}:ThCl_4$

Fig. 3 : f-d transitions in $Pa^{4+}:ThBr_4$

Fig. 4 : Polarized spectra of $U^{4+}:ThCl_4$ and $U^{4+}:ThSiO_4$ in the visible region

Fig. 5 : Absorption spectra of $U^{4+}:ThCl_4$ and UCl_4 in the visible region

Fig. 6 : Energy levels diagram for $U^{4+}:ThBr_4$
(P. Delamoye, Ph.D. Thesis, Université Paris-Sud 1985)

Fig. 7 : Energy levels diagram for $Np^{4+}:ThSiO_4$
(M.P. Lahaile, Ph.D. Thesis, Université Paris-Sud 1986)

Fig. 8 : $Pu^{4+}:ThSiO_4$ polarized absorption spectra in the visible range - the absorption of Pu^{4+} in $DClO_4$ is reported in grey for comparison

Fig. 9 : An^{4+} energy levels diagram based on the predictive model (from W.T. Carnall and H.M. Crosswhite [11])

Fig. 10: Energy levels diagram for U^{V}, U^{4+}aquo and U^{4+} in $ThBr_4$ (from [11])

Fig. 11: Variation of the experimental values of the F^2, slater parameter for Ln^{3+}, An^{3+} and An^{4+} versus Z

Fig. 12: Variation of the experimental spin orbit constant values versus Z, for the An^{4+} and Ln^{3+}. The pseudo relativistic Hartree-Fock calculated values for An^{V} are reported for comparison

Fig. 13: Comparison of the crystal field splitting of the ground-state manifold of lanthanide and actinide ions with the same f^n configuration

Fig. 14: Comparison of the splitting of the two lowest terms for the f^3 configuration of Nd^{3+} and Np^{4+} in D_{2d} symmetry

Z	Element	Electronic configurations				Element	Z
		An°	An^{3+}	An^{4+}	Ln^{3+}		
90	Th	$6d^2\ 7s^2$	$5f^1\ (^2F_{5/2})$				
91	Pa	$5f^2\ 6d\ 7s^2$	$5f^2\ (^3H_4)$	$5f^1\ (^2F_{5/2})$	$4f^1\ (^2F_{5/2})$	Ce	58
92	U	$5f^3\ 6d\ 7s^2$	$5f^3\ (^4I_{9/2})$	$5f^2\ (^3H_4)$	$4f^2\ (^3H_4)$	Pr	59
93	Np	$5f^4\ 6d\ 7s^2$	$5f^4\ (^5I_4)$	$5f^3\ (^4I_{9/2})$	$4f^3\ (^4I_{9/2})$	Nd	60
94	Pu	$5f^6\ 7s^2$	$5f^5\ (^6H_{5/2})$	$5f^4\ (^5I_4)$	$4f^4\ (^5I_4)$	Pm	61
95	Am	$5f^7\ 7s^2$	$5f^6\ (^7F_0)$	$5f^5\ (^6H_{5/2})$	$4f^5\ (^6H_{5/2})$	Sm	62
96	Cm	$5f^7\ 6d\ 7s^2$	$5f^7\ (^8S_{7/2})$	$5f^6\ (^7F_0)$	$4f^6\ (^7F_0)$	Eu	63
97	Bk	$5f^8\ 6d\ 7s^2$	$5f^8\ (^7F_6)$	$5f^7\ (^8S_{7/2})$	$4f^7\ (^8S_{7/2})$	Gd	64
98	Cf	$5f^{10}\ 7s^2$	$5f^9\ (^6H_{15/2})$	$5f^8\ (^7F_6)$	$4f^8\ (^7F_6)$	Tb	65
99	Es	$5f^{11}\ 7s^2$	$5f^{10}\ (^5I_8)$	$5f^9\ (^6H_{15/2})$	$4f^9\ (^6H_{15/2})$	Dy	66
100	Fm	$5f^{12}\ 7s^2$	$5f^{11}\ (^4I_{15/2})$	$5f^{10}\ (^5I_8)$	$4f^{10}\ (^5I_8)$	Ho	67
101	Md	$5f^{13}\ 7s^2$	$5f^{12}\ (^3H_6)$	$5f^{11}\ (^4I_{15/2})$	$4f^{11}\ (^4I_{15/2})$	Er	68
102	No	$5f^{14}\ 7s^2$	$5f^{13}\ (^2F_{7/2})$	$5f^{12}\ (^3H_6)$	$4f^{12}\ (^3H_6)$	Tm	69
103	Lr	$5f^{14}\ 6d\ 7s^2$	$5f^{14}\ (^1S_0)$	$5f^{13}\ (^2F_{7/2})$	$4f^{13}\ (^2F_{7/2})$	Yb	70
					$4f^{14}\ (^1S_0)$	Lu	71

Table 1

Configurations	Terms ^{2s+1}L	Number of J levels $^{2s+1}L_J$	Maximum number of crystal-field levels
f^1 and f^{13}	^2F	2	14
f^2 and f^{12}	^1SDGI ^3PFH	13	91
f^3 and f^{11}	$^2PDFGHIKL$ 2 2 2 2 ^4SDFGI	41	364
f^4 and f^{10}	$^1SDFGHIKLN$ 2 4 4 2 1 2 $^3PDFGHIKLM$ 3 2 4 3 4 2 2 ^5SDFGI	107	1001
f^5 and f^9	$^2PDFGHIKLMNO$ 4 5 7 6 7 5 5 3 2 $^4SPDFGHIKLM$ 2 3 4 4 3 3 2 ^6PFH	193	2002
f^6 and f^8	$^1SPDFGHIKLMNQ$ 4 6 4 8 4 7 3 4 2 2 $^3PDFGHIKLMNO$ 6 9 7 9 6 6 3 3 $^5SPDFGHIKL$ ^7F 3 2 3 2 2	295	3003
f^7	^2S P D F G H I K L M N O Q 2 5 7 10 10 9 9 7 5 4 2 $^4SPDFGHIKLMN$ 2 2 6 5 7 5 5 3 ^6PDFGHI ^8S	327	3432

Table 2

J integer			J half-integer		
C_n	Singlet	Doublet	Kramers - Doublet		
Twofold axis	μ = ± 0 , ± 1		1/2		
Threefold axis	± 0	1	1/2	3/2	
Fourfold axis	± 0 , ± 2	1	1/2	3/2	
Sixfold axis	± 0 , ± 3	1,2	1/2	3/2	5/2

Table 3

	Interactions	Hamiltonians	Parameters	Labels	Quantum numbers
Dominant interactions free-ion hamiltonian	Core potential	$H_0 = p^2/2m$		Configuration	n , ℓ
	Electronic repulsion ($n \geq 2$)	$H_{ER} = \sum_{k=0}^{6} f_k F^k$ (k even)	F^0 , F^2 F^4 , F^6	Terms	L , S
	Spin-orbit	$H_{so} = A_{so} \zeta_f$	ζ	J levels (free-ion)	L , S , J
Higher-order corrections free-ion hamiltonian	Two-body configuration interaction	$H_1 = \alpha L(L+1) + \beta G(G_2) + \gamma G(R_7)$	α, β, γ		
	Three-body configuration interaction ($n \geq 3$)	$H_2 = \sum_k t_k T^k$	T^k ($k=2,3,4,6,7,8$)		
	Magnetic effect due to configuration interaction	$H_3 = \sum_k p_k P^k$	P^k ($k = 2,4,6$)		
	Spin-spin and spin-other orbit	$H_4 = \sum_k m_k M^k$	M^k ($k = 0,2,4$)		
Ion in solid state	Crystal field interaction	$V_{CF} = \sum_{k,q,i} B^k_q (C^k_q)_i$	B^k_q k,q depend on site symmetry	crystal-field levels	μ

Table 4

	$Pa^{4+}:ThCl_4$		$Pa^{4+}:ThBr_4$		
L-S State	Obs. (cm^{-1})	Calc. (cm^{-1})	Obs. (cm^{-1})	Calc. (cm^{-1})	Irreducible Representation
$^2F_{5/2}$	0	21.8	0	19.9	Γ_6
	423	408.8	322	313.9	Γ_7
	1260	1252.7	954	940.5	Γ_6
$^2F_{7/2}$	5338	5312.4	5344	5324.3	Γ_6
	5590	5605.8	5517	5522.6	Γ_7
	6286	6291.3	6021	6026.0	Γ_6
	6711	6715.1	6458	6464.8	Γ_7

Table 5

Spectroscopic Parameters[a,b]	$Pa^{4+}:ThCl_4$ (44) (cm^{-1})	$Pa^{4+}:ThBr_4$ (44) (cm^{-1})
ξ	1524.2 (5)	1532.8 (5)
B_0^2	-1404.8 (50)	-1046.5 (52)
B_0^4	1749.4 (94)	1366.3 (138)
B_4^4	-2440.3 (98)	-1990.1 (102)
B_0^6	-2404.2 (607)	-1162.0 (541)
B_4^6	-194.5 (267)	623.1 (174)

[a]Root mean square = 23.6 cm^{-1} for $Pa^{4+}:ThCl_4$ and 19.4 cm^{-1} for $Pa^{4+}:ThBr_4$.

[b]These sets of parameters are obtained for F^0 = 3658 cm^{-1} for $Pa^{4+}:ThCl_4$ and F^0 = 3516 cm^{-1} for $Pa^{4+}:ThBr_4$.

Table 6

Table 7

Spectroscopic parameters[a]	$ThSiO_4 : U^{4+}$ (59)	$ThCl_4 : U^{4+}$ [b] (60)	UCl_4 [b] (61)	$ThBr_4 : U^{4+}$ [b] (46)
F^2	43110 (245)	42752 (162)	42561 (235)	42253 (127)
F^4	40929 (199)	39925 (502)	39440 (634)	40458 (489)
F^6	23834 (639)	24519 (479)	24174 (185)	25881 (383)
F^4/F^2	0.95	0.93	0.93	0.96
F^6/F^2	0.55	0.57	0.57	0.61
ζ	1840 (2)	1808 (8)	1805 (8)	1783 (7)
α	32.3 (0.4)	30.4 (2)	30.9 (1)	31 (1)
β	- 663 (144)	- 492 (84)	- 576 (168)	- 644 (75)
γ	(1200)	(1200)	(1200)	(1200)
B_0^2	- 1003 (127)	- 1054 (117)	- 903 (151)	- 1096 (80)
B_0^4	1147 (281)	1146 (200)	766 (220)	1316 (146)
B_4^4	- 2698 (251)	- 2767 (147)	- 3091 (185)	- 2230 (85)
B_0^6	- 2889 (557)	- 2135 (404)	- 1619 (482)	- 3170 (379)
B_4^6	- 208 (333)	- 312 (227)	- 308 (280)	686 (246)
$N_v(4\pi)^{-1/2}$ c)	1342	1256	1224	1340
η [d]	25	25	26	26
σ [d]	71	46	60	36

a) All parameters except γ vary

b) $M^0 = 0.99$; $M^2 = 0.55$; $M^4 = 0.38$; $P^2 = P^4 = P^6 = 500$

c) $N_v(4\pi)^{-1/2} = (\Sigma_k(1/2k + 1)\ (B_q^k)^2)^{1/2}$

d) r.m.s. $\sigma = (\Sigma_{i=0}^{n}\ \Delta_i^2/n-m)^{1/2}$ where Δ_i is the difference between the calculated and observed energy level, n is the number of observed levels and m the number of varying parameters.

		in D_{2d} symmetry		in D_2 symmetry	
Spectroscopic parameters	U^{V} (33) free-ion	$ThBr_4$-U^{4+} (46)	$ThCl_4$-U^{4+} (60)	$ThBr_4$-U^{4+} (46)	$ThCl_4$-U^{4+} (60)
F^2	51 938 (39)	42 253 (127)	42 752 (162)	42 264 (84)	42 736 (175)
F^4	42 708 (100)	40 458 (489)	39 925 (502)	41 159 (407)	39 821 (589)
F^6	27 748 (68)	25 891 (383)	24 519 (479)	26 018 (237)	24 438 (470)
ζ	1 968 (2)	1 783 (7)	1 808 (8)	1 774 (5)	1 805 (9)
α	33.5(0.4)	31 (1)	30.4 (2)	[31]	31.6 (2.2)
β	- 644 (25)	- 644 (75)	- 492 (84)	[644]	[- 492]
γ	744 (26)	[1 200]	[1 200]	[1 200]	[1 200]
M^0		[0.99]	[0.99]	[0.99]	[0.99]
M^2		[0.55]	[0.55]	[0.55]	[0.55]
M^4		[0.38]	[0.38]	[0.38]	[0.38]
P^2	573 (66)	[500]	[500]	[500]	[500]
P^6	524 (144)	[500]	[500]	[500]	[500]
P^4	1 173 (321)	[500]	[500]	[500]	[500]
B^2_0		- 1 096 (80)	- 1 054 (117)	- 1 108 (65)	- 1 037 (137)
B^4_0		1 316 (146)	1 146 (200)	1 358 (137)	1 121 (303)
B^4_4		- 2 230 (85)	- 2 767 (147)	- 2 219 (76)	- 2 948 (169)
B^6_0		- 3 170 (379)	- 2 135 (404)	- 3 458 (267)	- 2 120 (419)
B^6_4		686 (246)	- 312 (227)	694 (195)	- 315 (356)
B^2_2				- 78 (30)	- 77 (48)
B^4_2				318 (122)	356 (167)
B^6_2				136 (101)	158 (171)
B^6_6				123 (125)	424 (220)
n	13	26	25	38	34
σ	10	36	46	39	56

TABLE 8 : All parameters in square brackets are help constant.

Spectroscopic parameters	$U(BD_4)_4/Hf(BD_4)_4$ T_d site symmetry (67)	UCl_6^{2-} O_h site symmetry (68)	
F^2	41 280 (175)	41 175	42 266 (760)
F^4	40 013 (826)	40 838	39 604(3331)
F^6	22 554 (625)	28 858	26 360(2017)
ζ	1 782 (12)	1 792	1 760 (28)
α	38 (2)	[31]	
β	[648]	[644]	
γ	[1 200]	[1 200]	
M^0	[0.99]	[0.99]	
M^2	[0.55]	[0.55]	
M^4	[0.38]	[0.38]	
P^2	[500]	[500]	
P^4	[500]	[500]	
P^6	[500]	[500]	
B_0^4	- 2445 (124)	656	7 797 (394)
B_0^6	- 5371 (81)	1 472	1 344 (230)
No. of levels	19	23	23
σ	52	> 150	189
$N\nu/4\pi$	4 346		3 562

Table 9

All parameters in square brackets held constant.

For T_d or O_h symmetry, $B_4^4 = (5/14)^{1/2} B_0^4$, $B_4^6 = -(7/2)^{1/2} B_0^6$.

Table 10

Spectroscopic parameters	Np^{4+} : $ThSiO_4$ D_{2d} (74)	Np^{4+} : $ZrSiO_4$ D_{2d} (77)	$Np(BD_4)/Zr(BD_4)_4$ T_d (78)	Np^{4+}: ThO_2 O_h(Cubic) (74)
F^2	45196 (716)	46259	46689 (415)	49269 (968)
F^4	38032 (546)	44193	43239 (645)	37662 (1080)
F^6	28343 (791)	25463	26303 (722)	30937 (1434)
ζ	2129 (7)	2076	2089 (10)	2175 (13)
α	15 (3)		40 (2)	18 (3)
β	[- 600]		[- 600]	[- 600]
γ	[1200]		[1200]	[1200]
B_0^2	323 (185)	- 2104		
B_0^4	1511 (278)	4434	- 2722 (182)	- 854 (281)
B_4^4	- 3559 (163)	- 5251		
B_0^6	- 1871 (372)	- 4879	- 5070 (69)	- 994 (142)
B_4^6	- 801 (197)	- 79		
No.of levels	29	37	46	16
σ	47	75	84	74

In T_d or O_h symmetry $B_4^4 = (5/14)^{1/2} B_0^4$, $B_4^6 = -(7/2)^{1/2} B_0^6$. For all calculations, the values of the parameters $M^0 = 0.88$, $M^2 = 0.49$, $M^4 = 0.34$, $P^2 = P^4 = P^6 = 500$, $T^2 = 278$, $T^3 = 44$, $T^4 = 64$, $T^6 = -361$, $T^7 = 434$, and $T^8 = 353$ cm^{-1} were used. Values in square brackets were held constant. All parameters are in cm^{-1}.

	U^{3+}	Np^{3+}	Pu^{3+}	Am^{3+}	Cm^{3+}	Bk^{3+}	Cf^{3+}	Es^{3+}
F^2(HFR)[a]	71 442	74 944	78 223	81 346	84 331	87 192	89 964	92 657
F^2(FIT)[b]	39 715	44 907	48 670	51 800	55 109	57 015	61 014	62 766
Difference	31 727	30 037	29 553	29 546	29 222	30 177	28 950	29 891
F^4(HFR)	46 370	48 733	50 942	53 044	55 049	56 969	58 826	60 629
F^4(FIT)	33 537	36 918	39 188	41 440	43 803	45 698	44 483	48 003
Difference	12 833	11 815	11 754	11 604	11 246	11 271	14 343	12 626
F^6(HFR)	33 918	35 684	37 335	38 905	40 403	41 826	43 222	44 567
F^6(FIT)	23 670	25 766	27 493	30 050	32 610	33 552	36 168	35 309
Difference	10 248	9 918	9 842	8 855	7 793	8 274	7 054	9 258
ζ(HFR)	1 898	2 182	2 479	2 792	3 119	3 463	3 824	4 023
ζ(FIT)	1 623	1 938	2 241	2 580	2 903	3 216	3 568	3 962
Difference	275	244	238	212	216	247	256	241

Table 11 : a. Computed using Hartree-Fock methods and including an approximate relativistic correction [90,6]

b. Computed by fitting to experimental data.

	U^{4+}	Np^{4+}	Pu^{4+}	Am^{4+}	Cm^{4+}	Bk^{4+}	Cf^{4+}	Model Value
F^2(HFR)[b]	76 724	79 892	82 960	85 817	88 625	91 338	93 984	
F^2(Est)[c]	42 918	46 090	49 110	52 020	54 825	57 540	60 185	
Difference	33 806	33 802	33 798	33 797	33 800	33 798	33 799	33 800
F^4(HFR)	50 199	52 330	54 356	56 307	58 188	60 003	61 772	
F^4(Est)	39 873	42 000	44 030	45 980	47 860	49 670	51 440	
Difference	10 326	10 330	10 326	10 327	10 328	10 333	10 332	10 330
F^6(HFR)	36 860	38 452	39 965	41 423	42 827	44 181	45 500	
F^6(Est)	25 588	27 180	28 695	30 150	31 555	32 910	34 230	
Difference	11 272	11 272	11 270	11 273	11 272	11 271	11 270	11 270
ζ(HFR)	2 110	2 397	2 697	3 014	3 347	3 697	4 064	
ζ(Est)	1 810	2 095	2 395	2 715	3 045	3 395	3 765	
Difference	300	302	302	299	302	302	299	300

Table 12 : a. *In addition to the free-ion parameters shown, the following parameter values (in cm^{-1}) were used in all calculations :*
α = 30.12, β = - 660, γ = 1 200, B_0^2 = - 1 129, B_0^4 = 1793,
B_4^4 = - 2 617, B_0^6 = 3 016, B_4^6 = 342.
p^2 = 500, p^4 = 375, p^6 = 250. For $5f^N$ where N ≥ 3,
threebody parameters were included and the values assigned were :
T^2 = 200, T^3 = 50, T^4 = 100, T^6 = - 300, T^7 = 400, T^8 = 350.

b. Computed using Hartree-Fock methods and including and approximate relativistic correction [90,6].

c. Parameter value used to compute the energy level structure.
The set for U^{4+} was estimated for U^{4+} : $ThCl_4$ [60].

spectroscopic parameters	$ThCl_4 : Pr^{3+}$ [94] Set 1	$ThCl_4 : Pr^{3+}$ [94] Set 2	$ThBr_4 : Pr^{3+}$ [95]	$LuPO_4 : Pr^{3+}$ [96]	$YPO_4 : Pr^{3+}$ [96]	$ThBr_4 : U^{4+}$ [46]	$ThCl_4 : U^{4+}$ [60]
F^2	67 947	67 866	68 354	67 688	67 779	42 253	42 752
F^4	50 576	50 219	50 310	48 633	49 603	40 458	39 925
F^6	33 468	33 322	33 799	32 151	32 413	25 881	24 519
ζ	742	742	739	744	739	1 783	1 808
α	21	19	21	21	21	31	30
$\beta/12$	-39	-43	-67	-55	-55	-54	-41
γ	1 343	1 343	1 343	1 534	1 534	1 200	1 200
B_0^2	545	20	260	21	78	-1 096	-1 054
B_0^4	-657	292	-644	280	321	1 316	1 146
B_4^4	876	-964	929	-808	-849	-2 230	-2 767
B_0^6	1 398	-1 525	1 089	-1 658	-1 377	-3 170	-2 135
B_4^6	508	52	241	291	35	686	- (312)
Number of levels	52	52	42	18	35	26	25
σ (cm^{-1})	34	66	61	27	15	36	46

Table 13

Complex	$\beta = \frac{P^2 \text{ (crystal)}}{P^2 \text{ (free ion)}}$	$= \frac{B \text{ (crystal)}}{B \text{ (free ion)}}$	References
$U(BD_4)_4$ in $Uf(BD_4)_4$	0.79		67
Cs_2UX_6 (X = Br)	0.80		54
(X = Cl)	0.81		54
$ThSiO_4 : U^{4+}$	0.83		59
$ThX_4 : U^{4+}$ (X=Br)	0.81		46
(X=Cl)	0.92		60
UCl_4	0.82		61
$LaCl_3 : Pr^{3+}(4f^2)$	0.93		6
$Cr^{3+}(3d^3)$ in K_2NaCrF_6		0.83	97

Table 14

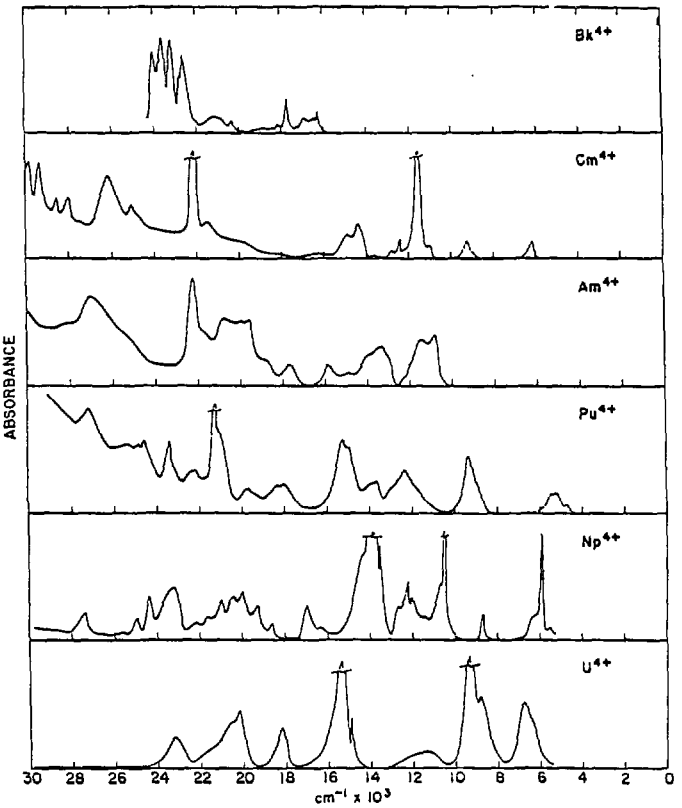
Bk4+
Cm4+
Am4+
Pu4+
Np4+
U4+
ABSORBANCE
30 28 26 24 22 20 18 16 14 12 10 8 6 4 2 0
cm-1 x 10³

FIGURE 1

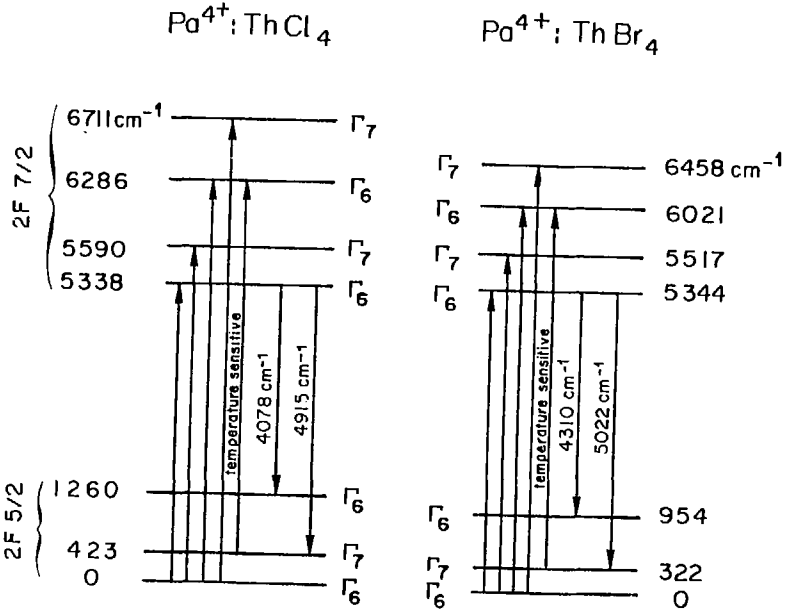
Pa^{4+} : $ThCl_4$
Pa^{4+} : $ThBr_4$
2F 7/2
2F 5/2
6711cm^{-1}
6286
5590
5338
1260
423
0
Γ_7
Γ_6
Γ_7
Γ_6
Γ_6
Γ_7
Γ_6
temperature sensitive
4078 cm^{-1}
4915 cm^{-1}
6458 cm^{-1}
6021
5517
5344
954
322
0
temperature sensitive
4310 cm^{-1}
5022 cm^{-1}

FIGURE 2

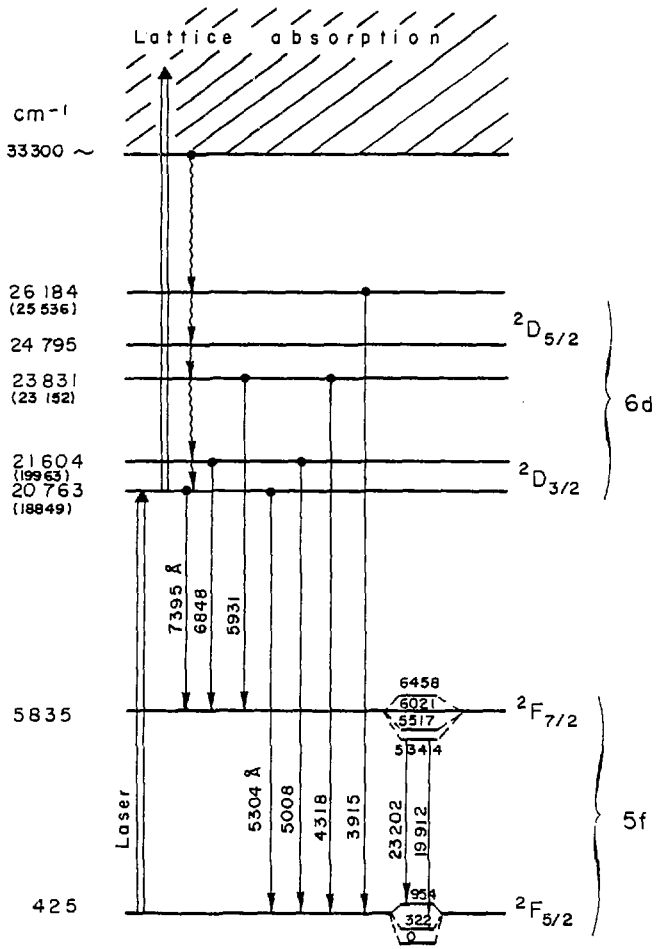

Fluorescence transitions in Pa^{4+} : $ThBr_4$

FIGURE 3

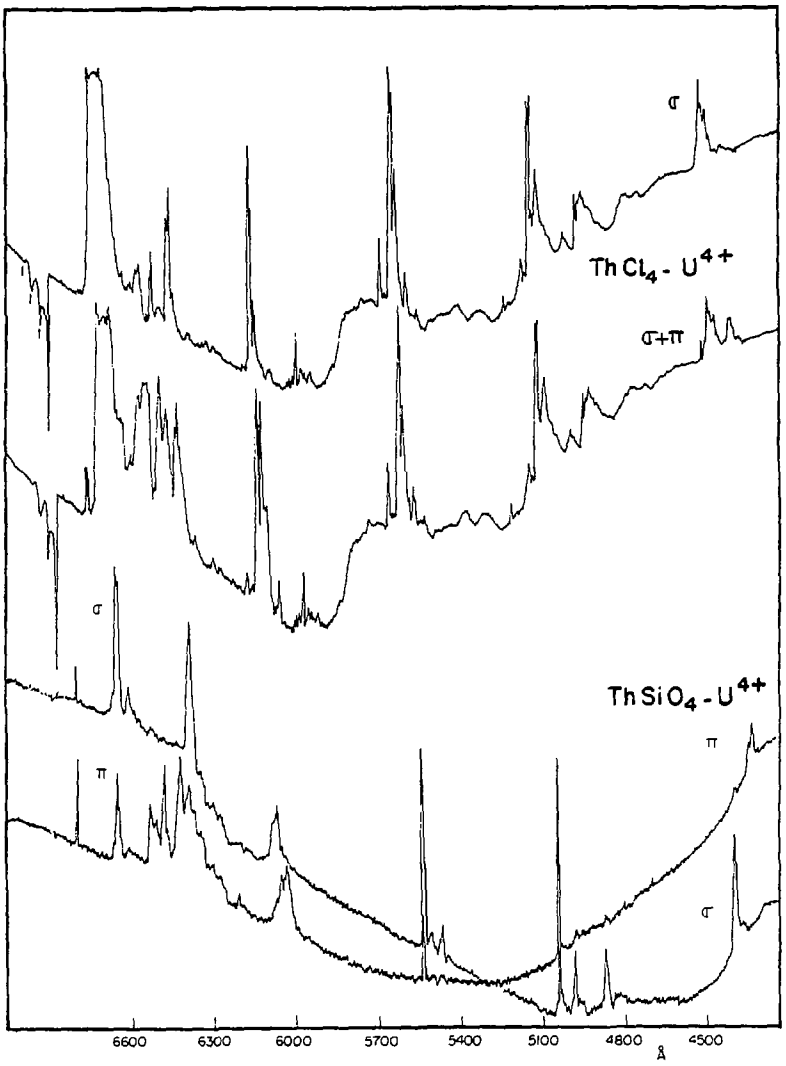
σ
$ThCl_4 - U^{4+}$
σ+π
σ
$ThSiO_4 - U^{4+}$
π
π
σ
6600
6300
6000
5700
5400
5100
4800
4500
Å

FIGURE 4

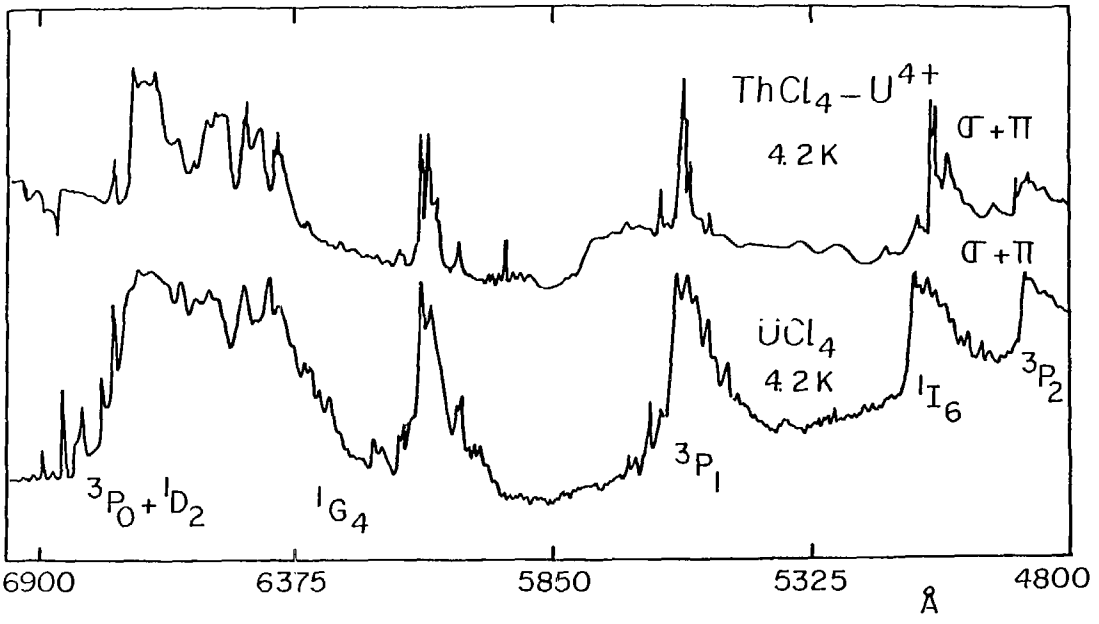
ThCl4 – U4+
4.2K
σ+π
σ+π
UCl4
4.2K
3P2
1I6
3P1
1G4
3P0+1D2
6900
6375
5850
5325
4800
Å

FIGURE 5

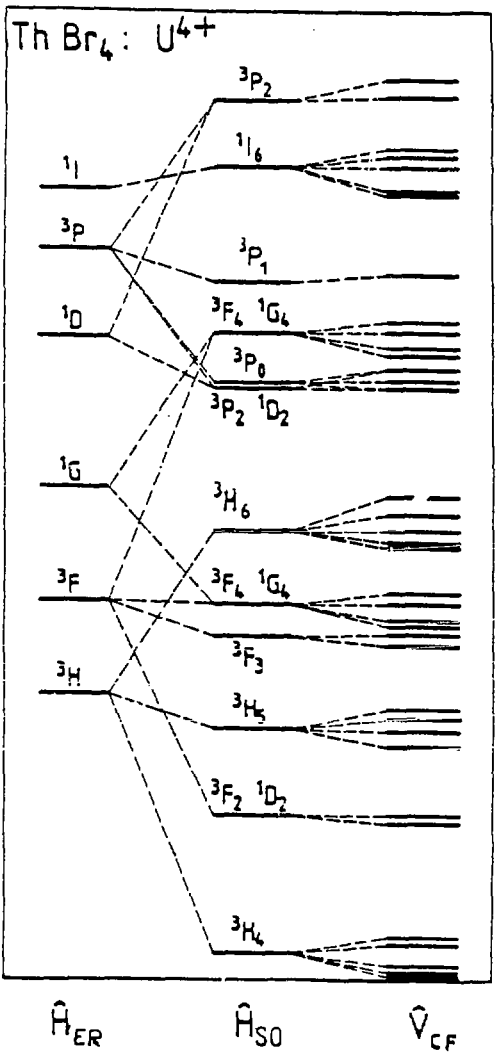
Th Br4 : U4+
3P2
1I6
1I
3P
3P1
1D
3F4 1G4
3P0
3P2 1D2
1G
3H6
3F
3F4 1G4
3F3
3H
3H5
3F2 1D2
3H4
ĤER
ĤSO
V̂CF

FIGURE 6

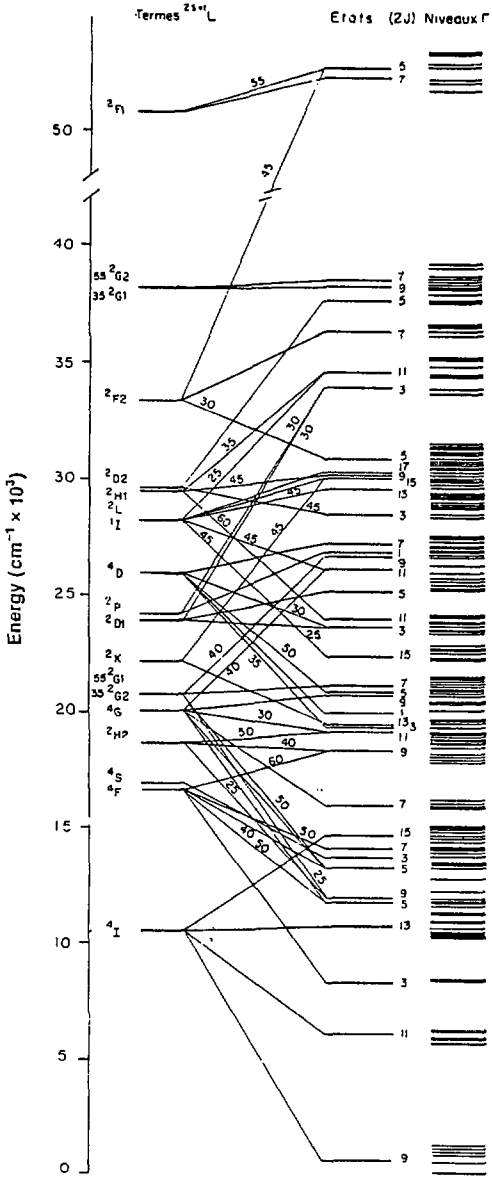
Termes ^{2S+1}L
Etats (2J)
Niveaux Γ
Energy (cm^{-1} x 10^3)
50
40
35
30
25
20
15
10
5
0
$^2F_1$
$^{55}\,^2G_2$
$^{35}\,^2G_1$
$^2F_2$
$^2D_2$
$^2H_1$
^2L
^1I
^4D
^2P
$^2D_1$
^2K
$^{55}\,^2G_1$
$^{35}\,^2G_2$
^4G
$^2H_2$
^4S
^4F
^4I

FIGURE 7

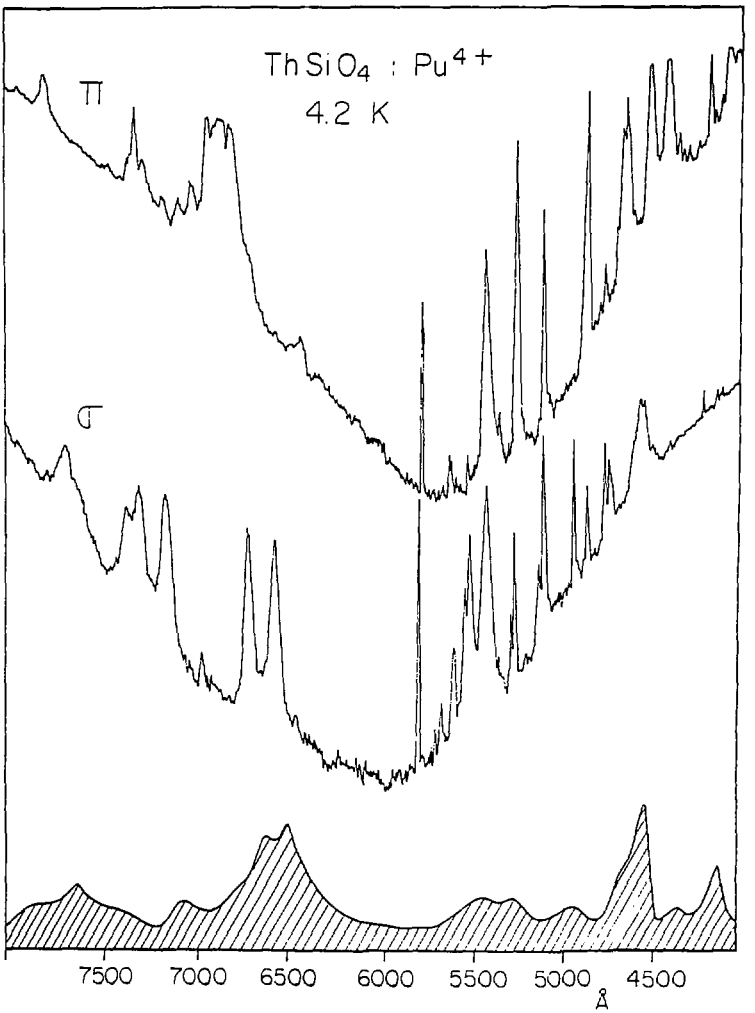

FIGURE 8

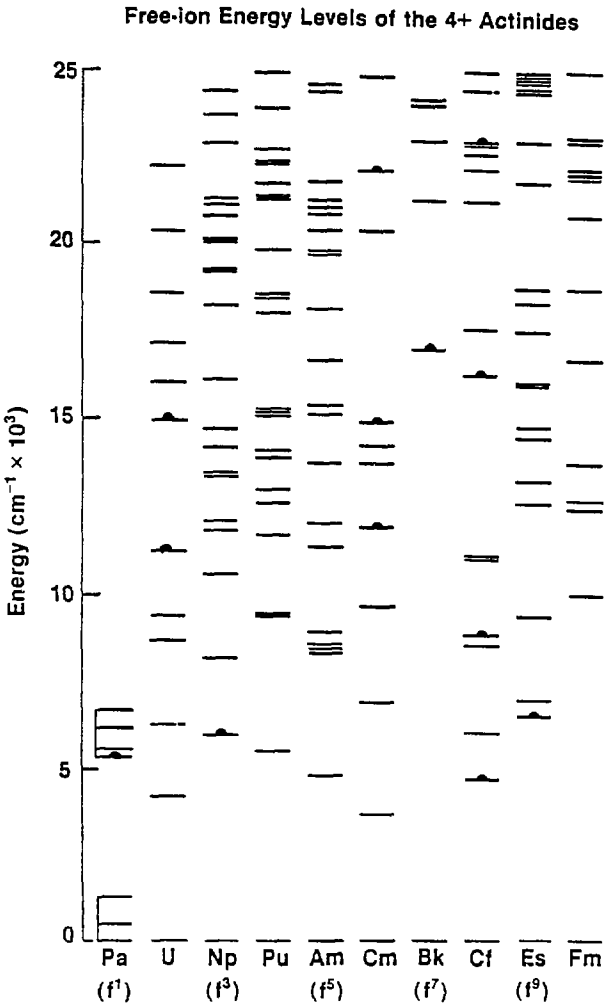
Free-ion Energy Levels of the 4+ Actinides
Energy (cm^{-1} × 10^3)
25
20
15
10
5
0
Pa
(f^1)
U
Np
(f^3)
Pu
Am
(f^5)
Cm
Bk
(f^7)
Cf
Es
(f^9)
Fm

FIGURE 9

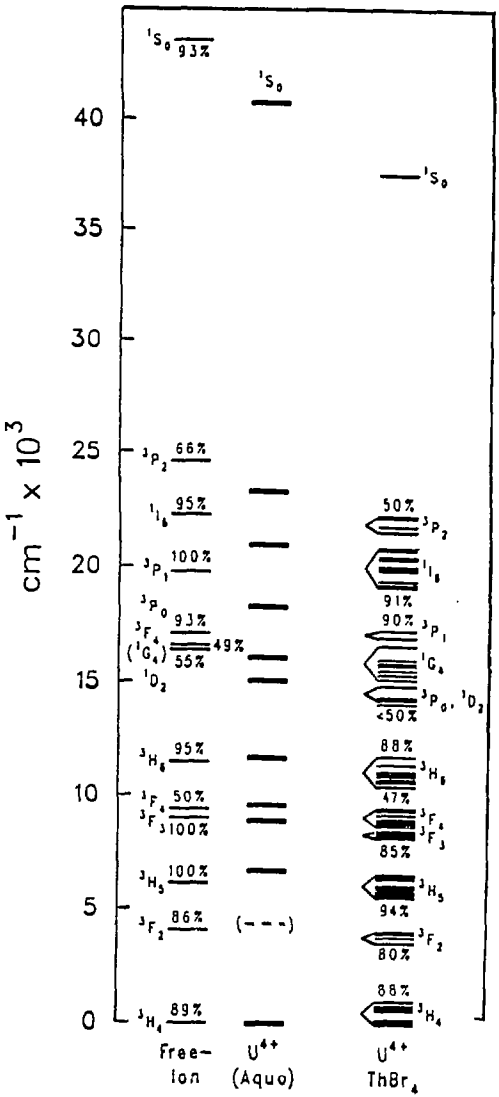
cm⁻¹ x 10³
40
35
30
25
20
15
10
5
0
¹S₀ 93%
¹S₀
¹S₀
³P₂ 66%
¹I₆ 95%
³P₁ 100%
³P₀ 93%
³F₄ (¹G₄) 49%
55%
¹D₂
³H₆ 95%
³F₄ 50%
³F₃ 100%
³H₅ 100%
³F₂ 86%
(- - -)
³H₄ 89%
50% ³P₂
¹I₆
91%
90% ³P₁
¹G₄
³P₀, ¹D₂
<50%
88% ³H₆
47%
³F₄
³F₃
85%
³H₅
94%
³F₂
80%
88% ³H₄
Free-ion
U⁴⁺ (Aquo)
U⁴⁺ ThBr₄

FIGURE 10

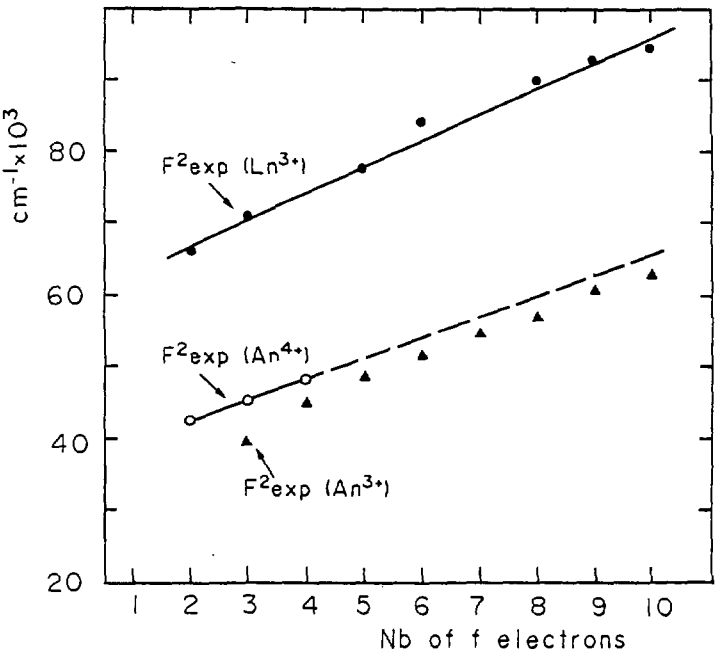
cm⁻¹x10³
80
60
40
20
F²exp (Ln³⁺)
F²exp (An⁴⁺)
F²exp (An³⁺)
1 2 3 4 5 6 7 8 9 10
Nb of f electrons

FIGURE 11

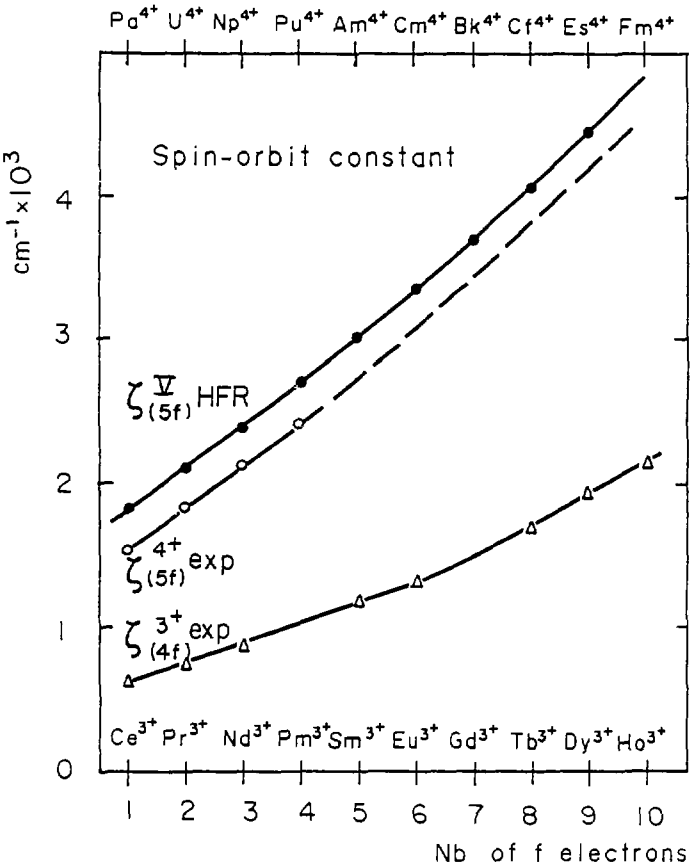
Pa4+ U4+ Np4+ Pu4+ Am4+ Cm4+ Bk4+ Cf4+ Es4+ Fm4+
Spin-orbit constant
cm-1 x 10^3
4
3
2
1
0
ζ V (5f) HFR
ζ 4+ (5f) exp
ζ 3+ (4f) exp
Ce3+ Pr3+ Nd3+ Pm3+ Sm3+ Eu3+ Gd3+ Tb3+ Dy3+ Ho3+
1 2 3 4 5 6 7 8 9 10
Nb of f electrons

FIGURE 12

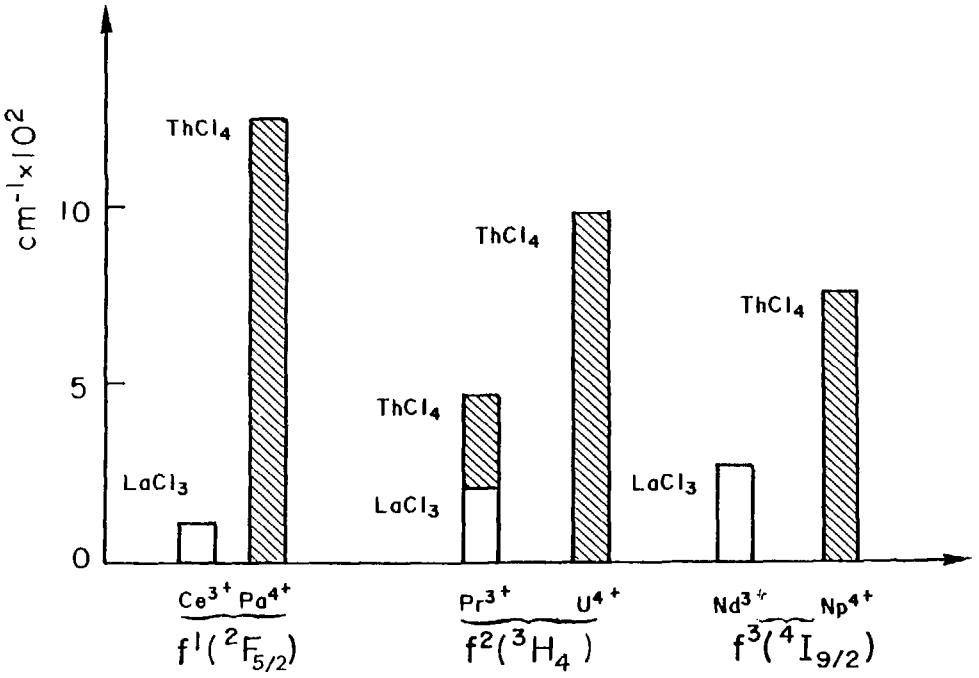
cm⁻¹×10²
10
5
0
ThCl4
LaCl3
ThCl4
LaCl3
ThCl4
LaCl3
ThCl4
Ce3+ Pa4+
f1(2F5/2)
Pr3+ U4+
f2(3H4)
Nd3+ Np4+
f3(4I9/2)

FIGURE 13

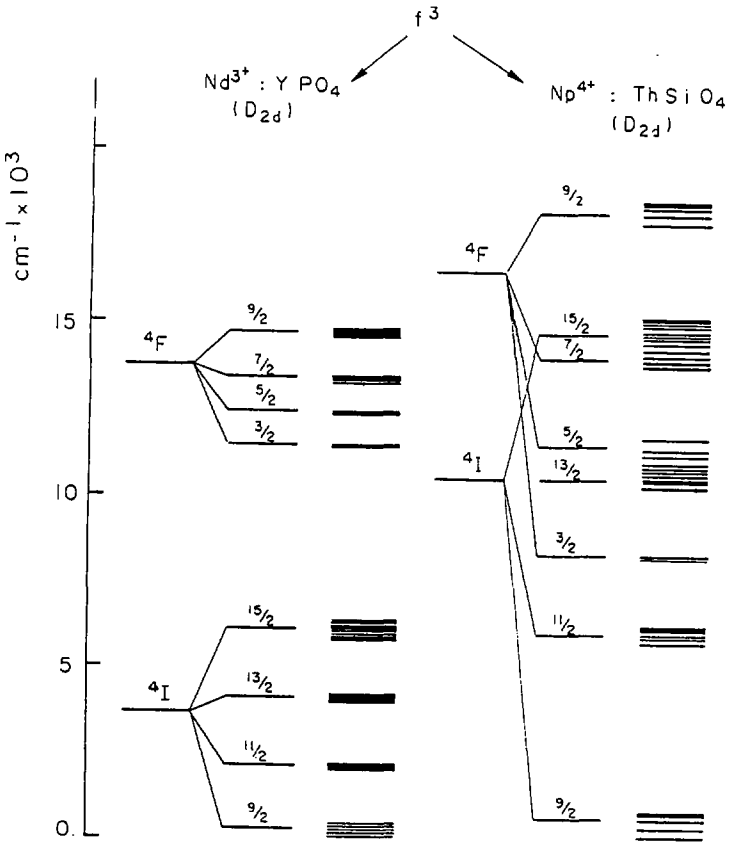
f 3
Nd3+ : Y PO4
(D2d)
Np4+ : Th Si O4
(D2d)
cm-1 x 10 3
15
10
5
0.
4F
4I
9/2
7/2
5/2
3/2
15/2
13/2
11/2
9/2

FIGURE 14